NASA TECHNICAL NOTE

NASA TN D-4909

NASA TN D-4909

EFFECTS OF ANGLE OF ATTACK AND BLUNTNESS ON THE SHOCK-LAYER PROPERTIES OF A 15° CONE AT A MACH NUMBER OF 10.6

by Joseph W. Cleary

Ames Research Center
Moffett Field, Calif.

NATIONAL AERONAUTICS AND SPACE ADMINISTRATION • WASHINGTON, D. C. • NOVEMBER 1968

EFFECTS OF ANGLE OF ATTACK AND BLUNTNESS ON THE SHOCK-LAYER PROPERTIES OF A 15° CONE AT A MACH NUMBER OF 10.6

By Joseph W. Cleary

Ames Research Center
Moffett Field, Calif.

NATIONAL AERONAUTICS AND SPACE ADMINISTRATION

For sale by the Clearinghouse for Federal Scientific and Technical Information
Springfield, Virginia 22151 – CFSTI price $3.00

EFFECTS OF ANGLE OF ATTACK AND BLUNTNESS ON THE SHOCK-LAYER PROPERTIES OF A 15° CONE AT A MACH NUMBER OF 10.6

By Joseph W. Cleary

Ames Research Center

SUMMARY

An experimental investigation was conducted to determine the effects of varying angle of attack and nose-bluntness ratio on the shock-layer properties of a typical conical entry body. Distributions of pitot and static pressures were measured across the shock layer of a cone with 15° semiapex. The measurements were obtained from wind-tunnel tests in air at a Mach number of 10.6 and a free-stream unit Reynolds number of 1.2×10^6 per foot. Results are presented at fore and aft axial positions for several circumferential angles when at angle of attack.

Pitot-pressure distributions demonstrate that the flow over the sharp cone was essentially conical except for the separated-flow region on the leeward side. Increasing bluntness ratio not only caused progressive deviations from conical flow but also affected the leeward flow-separation pattern. Comparisons with inviscid theory show that because of bluntness, the flow remained attached on the lee side for an axial distance of several nose radii while farther aft, the flow separated in a manner similar to that of the sharp cone. On the windward side where the boundary layer was thin, inviscid theory accurately predicts the more salient properties of shock layers for both sharp and blunted cones.

INTRODUCTION

Knowledge of the effects of angle of attack and bluntness on the distribution of flow properties in shock layers of conical bodies can be useful in the design of hypersonic vehicles that employ lift. Information on flow properties in shock layers is helpful to evaluate effects of flow asymmetry on convective heating, local flow separation, boundary-layer transition, and, as shown by the analysis of reference 1, the dynamics of entry bodies as well. For level-flight configurations, knowledge of effects of angle of attack and bluntness on shock-layer properties of the body may assist in the proper disposition of major components such as air inlets and stabilizing surfaces so that their effectiveness is optimized. While theoretical methods have been developed (refs. 2, 3, and 4, for example) to estimate inviscid flows when at angle of attack, viscous flows, in general, require experimental evaluation. The present experimental investigation presents measurements of shock-layer properties on a conical body that show effects of angle of attack and bluntness

for viscous flows. These results are an extension of those given in reference 5 and present in more complete form the preliminary results given in reference 6. Inviscid solutions of the flows are compared with experiment to indicate the significance of viscous effects and the limits of applicability of inviscid theory. Wind-tunnel measurements were made of pitot- and static-pressure distributions across the shock layer of a 15° semiapex cone. Angle-of-attack and cone-bluntness ratios were varied from 0° to 15° and 0 to 0.167, respectively. The free-stream Mach number was 10.6 and the free-stream unit Reynolds number was 1.2×10^6 per foot.

SYMBOLS

C_p	pressure coefficient, $\frac{p-p_\infty}{q_\infty}$
D	probe diameter
L	axial length of sharp cone
M	Mach number
p	pressure
q	dynamic pressure
R	nose radius
$\tilde{R}$	nose radius of bluntest model
Re*	unit Reynolds number
r_b	base radius of model
x,r,ϕ	cylindrical coordinates
α	angle of attack
γ	ratio of specific heats
δ	semiapex angle of cone
ζ	fraction of shock-layer thickness
ξ,η	surface coordinates along and perpendicular to body, respectively
θ	local shock angle
σ	conical angular coordinate between the shock and body axis
ψ	misalinement of the flow to the probe

Subscripts

min	minimum value
max	maximum value
p	pitot
s	static
∞	free stream

EXPERIMENTAL METHOD

Wind-Tunnel Facility

The tests were conducted in air in the Ames 3.5-foot hypersonic blowdown wind tunnel at a free-stream Mach number of 10.6 and a total temperature of 2000° R. Total pressure of the free stream was maintained at 1200 psia by a controller to provide a free-stream unit Reynolds number of 1.2×10^6 per foot. Although the free-stream flow had caloric imperfections, the effect of imperfections on pitot- and static-pressure coefficients is small and the test results can be considered essentially those for a perfect gas with $\gamma = 1.4$.

The model was sting supported at the base as shown in figure 1. The angle of attack ranged from 0° to 15°. The model angle of attack and free-stream total pressure were programmed into a controller prior to the test and the operation of the tunnel was essentially automatic. Data were recorded on magnetic tape. Other details of the wind-tunnel facility are given in reference 7.

Models and Test Procedure

The basic model (fig. 1) was a spherically blunted cone with a nose radius of 1 inch, a base radius of 6 inches and a semiapex of 15°. The model was constructed from stainless steel and had a wall thickness of 0.375 inch. Bluntness ratio R/r_b was varied by attaching nose tips having radii of 0.375 and 0 inch (sharp cone) that faired smoothly to the basic model at the sphere-cone tangent point.

The model was instrumented with pitot- and static-pressure probes connected to absolute-pressure cells of 50 and 10 psia capacity, respectively. The probes were mounted on fore and aft movable struts located on opposite sides of the model. Pitot and static pressures were measured during separate tests by interchanging probe and strut assemblies. The fore and aft struts supported two and three probes, respectively (fig. 1). Other details of the probes are given in figure 2. Traverses of the shock layer were made normal to the conical surface with the probes alined parallel to the cone generatrix.

The angular coordinate ϕ was varied in increments of 30° by an axial rotation of the model. The model was internally cooled, and the ratio of the surface temperature to free-stream total temperature was about 0.3.

Probe Interference and Flow Misalinement

Since the local Mach number within the shock layer was supersonic, the probe shock wave interacted with the boundary layer when the probe was near the conical surface. While the effects of this type of interaction on static-pressure measurements appeared generally small, significant increases of pitot pressure were observed locally, under certain conditions, on the windward side of the sharp cone. Apparently in regions of extreme shear, the pitot shock was either not normal or multiple shocks formed at the cone surface thereby causing greater pitot pressures. These data have been deleted since it was apparent for the sharp cone that the measurements were anomalous. Interference effects on pressure measurements from interaction of the strut shock with the boundary layer were investigated by means of an oil streak technique. Observations of local surface flow indicated that the probes were sufficiently long to prevent the shock-boundary-layer interaction from interfering with the pressure measurements. Moreover, it was apparent that the fore-strut wake did not interfere significantly with the flow over the aft probes. Significant interference was not apparent as the probes penetrated the shock wave from the model and pitot pressure decreased abruptly to the free-stream value.

Since the probes were alined with elements of the cone, misalinement to the local flow occurred during the traverses. For $\alpha = 0°$, the greatest misalinement ψ for the sharp cone occurred at the shock wave where $\psi = 2.5°$. This is believed insufficient to cause relevant effects on either pitot- or static-pressure measurements. However, because of cross flow, ψ increased with increasing angle of attack. To evaluate the importance of misalinement for $\alpha > 0°$, estimates of ψ were made from extrapolations of inviscid sharp-cone solutions of the flow given in reference 3. These estimates are shown in sketch (a) for $\alpha = 10°$. For the sharp cone, maximum ψ occurs at the shock for $\phi \approx 100°$ and is about equal in magnitude to the angle of attack.

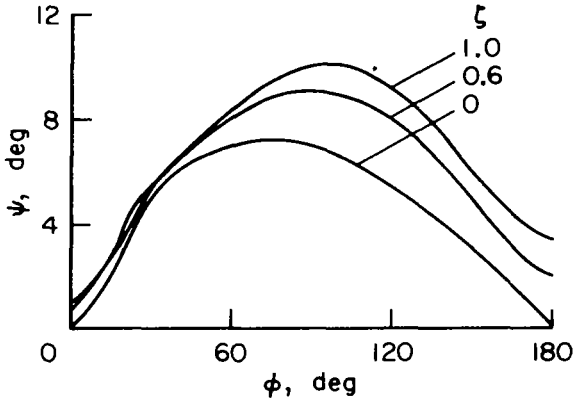

Sketch (a)

Estimates of flow misalinement for blunted cones by the method of reference 4 indicate that maximum ψ occurs at the cone surface and is about twice as great here as that for the sharp cone. However, these large values of ψ apply only to that part of the shock layer adjacent to the surface, and near the shock, ψ approaches the shock value for the sharp cone. To compensate partially for the effects of flow misalinement, static orifices were installed on the windward and leeward sides of the probes. However, because of the inherent difficulty in accurately measuring static pressure by an inclined probe, such measurements for large ψ are considered mainly of qualitative value. Pitot-pressure measurements, on the other hand, decrease very slowly with increasing ψ; reference 8 indicates that these measurements are valid even for $\psi \rightarrow 20°$. Since corrections to static-pressure measurements for flow misalinement, flow curvature, and viscous interaction were not known, the results are presented in uncorrected form.

Accuracy

At the lowest pressures measured, the precision of the pressure cells was about 1 percent of the measured pressure. However, because of inaccuracies in evaluating the free-stream Mach number, the precision of pressure coefficients is believed to be about ±2 to ±4 percent. Angle measurements are within ±0.2° and probe heights within ±0.02 inch.

RESULTS AND DISCUSSION

Locations of the fore and aft traverses with respect to characteristic dimensions of the cone are shown in figure 3. Note that the circumferential angle ϕ is measured from the most leeward conical ray. To simplify presentation of the results, the orientation of the windward side of the model has been inverted so that data for $\phi > 90°$ and $\alpha > 0°$ will be shown reflected in the model horizontal plane as if obtained for $\alpha < 0°$.

Experimental Results

Effects of angle of attack and bluntness on the distribution of shock-layer pitot and static pressures at the fore station, $x/L = 0.280$, are presented in figure 4. Similar results are given for the aft station $x/L = 0.784$ in figure 5. The ordinate η of these figures has been normalized by the nose radius of the bluntest model $\tilde{R}$ and the position of the shock wave is denoted by a horizontal bar whose length is proportional to bluntness. Shock-wave positions were estimated from the abrupt break in the distributions of pitot-pressure coefficient when the shock wave was penetrated by the pitots during the traverses. For some cases in lieu of pressure measurements near the shock, static-pressure curves have been extended to the value of static-pressure coefficient estimated by oblique-shock theory from the shock-wave position determined by the pitot traverse.

For a specified angle of attack, figures 4 and 5 show generally large effects of bluntness on the shock-layer pitot-pressure distributions. These effects are explained most simply by the results given for $\alpha = 0°$. At the aft station, figure 5(a) shows that for $\alpha = 0°$ the sharp-cone pitot pressure increases with increasing η/R as the boundary layer is traversed, and then decreases in a manner consistent with inviscid sharp-cone theory as the shock is approached from the boundary-layer edge. Bluntness altered this basic sharp-cone type pitot-pressure distribution by inducing a maximum whose shock-layer position relative to the cone surface increases with increasing bluntness. Similar effects of bluntness can be observed at the fore station (fig. 4(a)) except that for the bluntest cone ($R/r_b = 0.167$) pitot pressure has its greatest value at the shock and the distribution is similar to that predicted by blast-wave theory. These effects of bluntness are discussed in detail in references 5 and 6 where it is shown from inviscid solutions of the flow that the shock wave of blunted cones has an inflection resulting from the three-dimensional thinning of the entropy layer. If the traverse station is aft of the shock inflection, a maximum will occur in the pitot-pressure distribution; if the traverse station is forward, the pitot-pressure distribution resembles that given by blast-wave theory.

At a specified axial position, bluntness effects are significantly changed by increasing angle of attack. On the leeward side, figure 5(a) shows that for $R/r_b = 0.0625$, the pitot-pressure maximum approaches the shock and then vanishes as the shock inflection moves aft with increasing angle of attack. Conversely, an opposite effect of angle of attack can be observed on the windward side. As shown in figure 5(a) for $R/r_b = 0.167$, the pitot-pressure maximum approaches the cone surface as $\alpha \to -15°$. Absence of maxima for $R/r_b = 0.0625$ at $\alpha = -5°$ and $-10°$ at the aft traverse station is attributed to swallowing of the maxima by the boundary layer. Although a maximum is indicated for $\alpha = -15°$, this may result from probe interference (see Experimental Method section) because of the extremely thin boundary layer. Similar windward effects of angle of attack on pitot-pressure maxima can be seen in figure 4(a) at the fore station where the first appearance of a maximum for $R/r_b = 0.167$ is evident for $\alpha = -15°$. For $\alpha > 0°$ and particularly $\alpha = 15°$, attention is directed to the large effects of small bluntness ($R/r_b = 0.0625$) on pitot-pressure distributions at the fore station (fig. 4) for $\phi \leq 30°$ and the comparatively small effects for $\phi \geq 60°$. Apparently, the entropy layer was thinned sufficiently by cross flow that on the windward side effects of bluntness diminished within a few nose radii downstream, and at the aft traverse station (fig. 5), large effects of small bluntness are evident only for $\phi = 0°$.

Perhaps of equal importance to the aforementioned effects of bluntness are the effects on the thick boundary layers and separation patterns that occur on the lee side of sharp cones. From the sharp-cone traverses at $\phi = 0°$ (figs. 4(a) and 5(a)) it can be seen that the boundary layer thickened with increasing angle of attack. The abrupt change in pitot pressure midway in the shock layer at the higher angles of attack indicates (fig. 4(a)) that a shear surface formed midway in the shock layer. In addition, the sharp-cone pitot pressure at the cone surface is about the same as the static pressure. These facts and the observed invariance of the pitot pressure with increasing $\eta/\tilde{R}$ near the surface indicate that flow separation occurred at least for

$\alpha = 15°$. Furthermore, it is apparent from traverses for $\phi \geq 30°$ that the circumferential extent of the separated flow was less than 30°. Figure 4(a) shows that for $\alpha = 10°$ and 15°, bluntness alleviated the abrupt change in pitot pressure that characterizes the shear surface of the sharp cone. Adjacent to the cone surface, the greater pitot pressures for $R/r_b = 0.167$ than for lesser bluntness indicate that for this degree of bluntness the flow remained attached. Flow attachment effects of bluntness will be demonstrated more clearly later by comparisons with inviscid theory.

The effects of bluntness on static-pressure distributions were small compared to the previously observed effects on pitot-pressure distribution. Largest effects of bluntness on static-pressure distributions occurred at the fore station where it can be seen in figure 4 that on the leeward side of the bluntest cone (and also for $\alpha = 0°$) the pressure distributions resemble predictions by blast-wave theory. At the aft station, the distribution of static pressure on the lee side was essentially constant and unaffected by bluntness. Similarly, bluntness effects were generally small on the windward side, and for $\phi = 180°$, static pressure of the sharp and blunted cones decreased gradually as the shock was approached from the cone surface. Finally, it is of interest to note the large increase in shock-layer thickness on the lee side (figs. 4(a) and 5(a)) due to bluntness even though increasing bluntness tended to keep the flow attached.

Comparisons With Theory

Before showing comparisons of experimental shock-layer properties with theory, some aspects of the sharp-cone shock waves will be examined to determine the conical nature of the experimental results. Because of the high Reynolds number of the test, effects of shock-boundary-layer interaction on the conical nature of the flow were small. However, boundary-layer growth and subsequent flow separation on the leeward side might have an influence and it is appropriate to evaluate if the shock wave was similar at the fore- and aft-traverse stations.

Sharp-cone shock-wave properties.- Values of the conical coordinate $\sigma - \delta$ estimated from the fore and aft traverses are shown and compared with theory in figure 6. Here it can be seen that values of $\sigma - \delta$ from the fore traverses agree well with those from the aft traverses. Since the greatest difference between the fore and aft traverses is about 0.4°, it is clear that the sharp-cone shocks were essentially conical even at $\alpha = 15°$ for which leeward separation occurred. Theory shown in figure 6 for $\alpha = 0°$ is an inviscid solution of the flow by the method of characteristics while that for $\alpha = 5°$ and 10° is an extrapolation to $M_\infty = 10.6$ of numerically exact inviscid solutions given in reference 3 for the Mach number range 2 to 7. On the windward side, $\phi > 120$, figure 6 shows good agreement between theory and experiment. However, because of boundary-layer growth and subsequent flow separation, theory underestimated experiment for $0° \leq \phi \leq 120°$.

Assuming the shocks were conical, estimates were made of the local oblique-shock angles, θ, using the experimentally faired curves of $\sigma - \delta$ shown in figure 6. These estimates are compared with extrapolations of the

theory of reference 3 in figure 7. Good agreement between theory and experiment is shown for $0° \leq \alpha \leq 10°$ except on the lee side where viscous effects are important. In lieu of theoretical results for $\alpha = 15°$, a cosine distribution of θ given by equation (1) was assumed for comparative purposes.

$$\theta = \frac{\theta_{max} + \theta_{min}}{2} - \frac{\theta_{max} - \theta_{min}}{2} \cos \phi \qquad (1)$$

Experimental values of θ_{min} and θ_{max} were selected for $\phi = 0°$ and 180°, respectively, and used in equation (1) to compute the dashed curve shown in figure 7. It can be seen that the experimental shock angles are closely approximated by a cosine distribution of θ. (The inviscid solutions of ref. 3 also are closely approximated by a cosine distribution of θ.) It is concluded from these results that boundary-layer growth and subsequent flow separation did not have an unusual effect on shock shape even though separation may be abrupt and accompanied by imbedded shocks (refs. 9 and 10).

Sharp-cone shock-layer properties.- Experimental pitot- and static-pressure distributions from the fore and aft traverses of the sharp-cone shock layer are compared with theory in figure 8. The ordinate η has been normalized by the surface distance from the cone apex to the traverse station ξ so that pressure distributions are shown as functions of a conical coordinate. Except for the leeward separated-flow region, the distributions measured at the fore station agree well with those measured at the aft station (fig. 8), thus verifying that the shock-layer flow as well as the shock-wave shape was essentially conical. Agreement with theory is considered reasonably good, but some differences in details can be seen. For $\alpha = 0°$, theory is an exact inviscid solution of the flow by the method of characteristics, while that for $\alpha = \pm 5°$ and $\pm 10°$ is an extrapolation of inviscid solutions from reference 3. The veracity of the extrapolations has been substantiated by limited computations using the three-dimensional method-of-characteristics program described in reference 4. Although theoretical solutions were not available from reference 3 for comparison at $\alpha = \pm 15°$, the experimental results are shown for completeness. For $\alpha = 0°$, figure 8(a) shows that the measured static-pressure distribution agrees well with theory, as well as with the surface measurement shown by the shaded inverted triangular symbol. The pitot-pressure distribution also agrees well with theory, except for a slight difference in level, which can be seen in figure 8(a). Reasons for this difference are not known; however, since static pressure agrees well with theory, the differences of pitot pressure imply an increase of entropy. Similar differences exist for $|\alpha| > 0°$, except somewhat better agreement with theory is indicated on the windward side. Measurements of shock angle (fig. 6) afford an independent check of pitot pressure at the shock by oblique-shock theory and estimated values of pitot- and static-pressure coefficient by this theory are shown in figure 8 as half-shaded symbols. It can be seen that the oblique-shock estimates of pitot pressure are also greater than measured values but the oblique-shock static-pressure estimates agree well with measurements. On the windward side where the boundary layer was thin, the oblique-shock estimates differ very little from conical-flow theory as expected. Differences shown on the leeward side are, of course, associated with greater

experimentally observed shock angles. For $\phi = 0°$ (fig. 8(a)) and $\alpha = 15°$, the oblique-shock estimate of pitot-pressure coefficient is about 35 percent greater than measured. While this difference may seem large, it could accrue from only about 1.5° difference in shock angle. However, since the measured shock angles agree within about ±0.4°, it appears that the loss of pitot pressure may be associated with a slight entropy increase within the shock layer.

Observed differences between theory and measured pitot pressure adjacent to the cone surface are, of course, due to the boundary layer, since the theory is inviscid. Figure 8 shows that for $|\alpha| > 0°$ the thin entropy layer predicted by theory (as shown by a fairly abrupt decrease of pitot pressure adjacent to the surface for $30° \leq \phi \leq 150°$) was essentially swallowed by the boundary layer. Finally, from the measured pitot-pressure distributions at the fore and aft stations it can be seen in figure 8(a) that on the lee side for $\alpha = 10°$ and 15° the flow in the shock layer was not conical. Apparently, because of viscous dissipation and turbulent mixing, the thickness of the separated flow relative to that of the shock-layer thickness decreased with increasing axial distance. As can be seen from figure 8, however, this departure from conical flow was restricted to $\phi < 30°$.

Blunted-cone shock-layer properties.- Measured distributions of shock-layer pitot and static pressures will be compared first with an exact inviscid solution of the flow by the three-dimensional method of characteristics program of reference 4. Comparisons then are made with an approximate method that can be applied on leeward and windward rays. Since solutions of blunted-cone flows at angle of attack by the three-dimensional method of characteristics entail significant computing time, comparisons with this theory are limited to one angle of attack, $\alpha = 10°$. This comparison is shown in figure 9 for $R/r_b = 0.167$ at two axial stations. Note that traverse stations are measured from the nose and given in terms of nose radii (see fig. 3). Also, the theoretical solution is for $M_\infty = 10$ rather than the experimental value $M_\infty = 10.6$. This slight difference in Mach number between theory and experiment is irrelevant to static-pressure comparisons but because of it, the theoretical distribution of pitot-pressure coefficient is low by about 2 or 3 percent.

With minor exceptions, figure 9 shows generally good agreement between theory and experiment. At the fore station, $x/R = 3.4$, figure 9(a) shows that the measured pitot pressures agree closely with theory even on the lee side. Farther aft at $x/R = 14.7$ (fig. 9(b)), viscous effects on the lee side appear more prominent but the measured distributions of pitot pressure resemble those predicted by theory. On the windward side, viscous effects are small and it is noteworthy how closely details of the measured pitot-pressure distribution including the maximum pitot pressure and the shock position are predicted by theory. However, exceptions to this good agreement can be seen for example in the comparison of pitot- and static-pressure distributions with theory in figure 9(b) for $\phi = 120°$ and 180°, respectively. Here, anomalous differences arise mainly from a shift in level of the measured pressures that may be due to experimental inaccuracies.

Numerical difficulties associated with thinning of the entropy layer curtailed solving for the flow by the three-dimensional method of characteristics at a station forward of the most aft blunted-cone traverse, $x/R = 43.9$ (see fig. 3). Comparisons therefore are made with an approximate method designated the equivalent-body theory. This approximation has been shown previously (refs. 2 and 6) to yield adequate accuracy for preliminary comparisons. In essence, the flow at angle of attack is approximated by an equivalent axisymmetric flow over a blunted cone whose cone angle equals the surface inclination of the inclined blunted cone. Because of the effects of crossflow for large x/R, comparisons by this method are limited to the flow along leeward and windward rays only. However, since solutions of axisymmetric flow are achieved readily, comparisons are made for several angles of attack and axial stations.

Figure 10 shows a comparison of pitot- and static-pressure distributions predicted by equivalent-body theory with experiment. To assist in judging the adequacy of equivalent-body theory, figures 10(b) and 10(f) also show predictions presented previously for $\alpha = 10^\circ$ and $M_\infty = 10$ by the three-dimensional method of characteristics. These comparisons demonstrate that equivalent-body theory provides a good estimate of shock-layer properties for axial stations near the nose. At larger x/R, equivalent-body theory gives reasonable estimates of shock-layer properties but there are differences in details. If $\alpha = 0^\circ$, equivalent-body theory is, of course, the appropriate axisymmetric solution that can be compared with experiment to show viscous effects. For this case figure 10(d) indicates that at $x/R = 3.4$ the boundary layer was thin and theory agrees closely with experiment. For $x/R = 14.7$ and 43.9, on the other hand, theory slightly overestimated the distribution of pitot-pressure coefficient. On the windward side for $x/R = 43.9$, figure 10 shows that as $\alpha \to -15^\circ$ equivalent-body theory overestimates the distance to the shock and the level of static pressure, and tends to underestimate the distribution of pitot pressure. These shortcomings for large x/R are inherent in this method since it is basically a tangent-cone approximation. Leeward, figures 10(e) to 10(g) indicate that for $x/R = 3.4$ at least, the boundary layer was relatively thin and the flow remained attached as shown by the generally close agreement of pitot pressure with theory. However, with increasing x/R, agreement with theory is not as good and it is apparent that some measure of flow separation was incurred at $x/R = 43.9$.

CONCLUDING REMARKS

Experimental results demonstrate the more salient effects of varying nose-bluntness ratio on the shock-layer properties of a 15°-semiapex cone. Tests at angle of attack show that for $M_\infty = 10.6$ and $Re_\infty^* = 1.2 \times 10^6$ per foot the shock-layer properties of the sharp cone are essentially conical except for the separated flow on the lee side. Shock-layer pitot- and static-pressure distributions of the sharp cone agree reasonably well with inviscid conical flow theory.

Increasing bluntness ratio causes progressive departures of shock-layer properties from conical flow and alters the pattern of flow separation on the lee side. For large angles of attack the flow over the lee side of the blunted cone remains attached for several nose radii downstream before separation develops. When the flow was attached, inviscid theory adequately predicts the shock-layer properties of the blunted cone.

Ames Research Center
National Aeronautics and Space Administration
Moffett Field, Calif., 94035, Aug. 14, 1968
129-01-03-10-00-21

REFERENCES

1. Ericsson, L. E.: Effect of Nose Bluntness on the Hypersonic Unsteady Aerodynamics of an Ablating Re-Entry Body. J. Spacecraft Rockets, vol. 4, no. 6, June 1967.

2. Gallo, William F.; and Rakich, John V.: Investigation of Methods for Predicting Flow in the Shock Layer Over Bodies at Small Angles of Attack. NASA TN D-3946, 1967.

3. Babenko, K. I., et al.: Three-Dimensional Flow of Ideal Gas Past Smooth Bodies. NASA TT F-380, 1966.

4. Rakich, John V.: Three-Dimensional Flow Calculation by the Method of Characteristics. AIAA J., vol. 5, no. 10, Oct. 1967.

5. Cleary, Joseph W.: An Experimental and Theoretical Investigation of the Pressure Distribution and Flow Fields of Blunted Cones at Hypersonic Mach Numbers. NASA TN D-2969, 1965.

6. Cleary, Joseph W.: Effects of Angle of Attack and Nose Bluntness on the Hypersonic Flow Over Cones. AIAA Paper 66-414, 1966.

7. Holdaway, George H.; Polek, Thomas E.; and Kemp, Joseph H.: Aerodynamic Characteristics of a Blunt Half-Cone Entry Configuration at Mach Numbers of 5.2, 7.4, and 10.4. NASA TM X-782, 1963.

8. Liepman, H. W.; and Roshko, A.: Elements of Gasdynamics. GALCIT, Aeronautical Series, John Wiley and Sons, N. Y., 1957.

9. Tracy, R. R.: Hypersonic Flow Over a Yawed Circular Cone. Hypersonic Research Project Memo. 69, California Institute of Technology, Aug. 1963.

10. Rainbird, William J.: Turbulent Boundary Layer Growth and Separation on a Yawed 12-1/2° Cone at Mach Numbers 1.8 and 4.25. AIAA Paper 68-98, 1968.

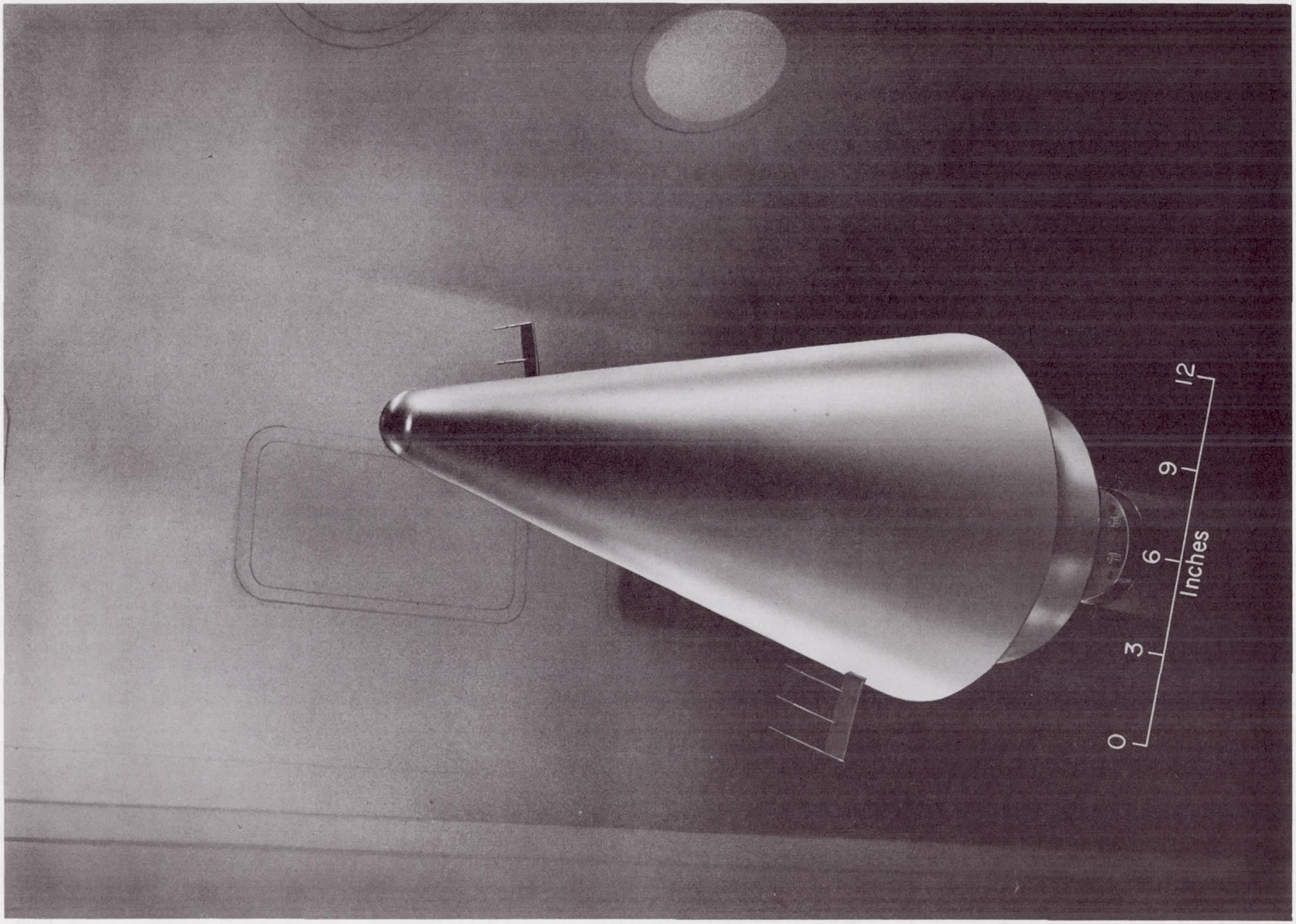

A-32127-12.1

Figure 1.- Model mounted on the sting support in the Ames 3.5-foot wind tunnel.

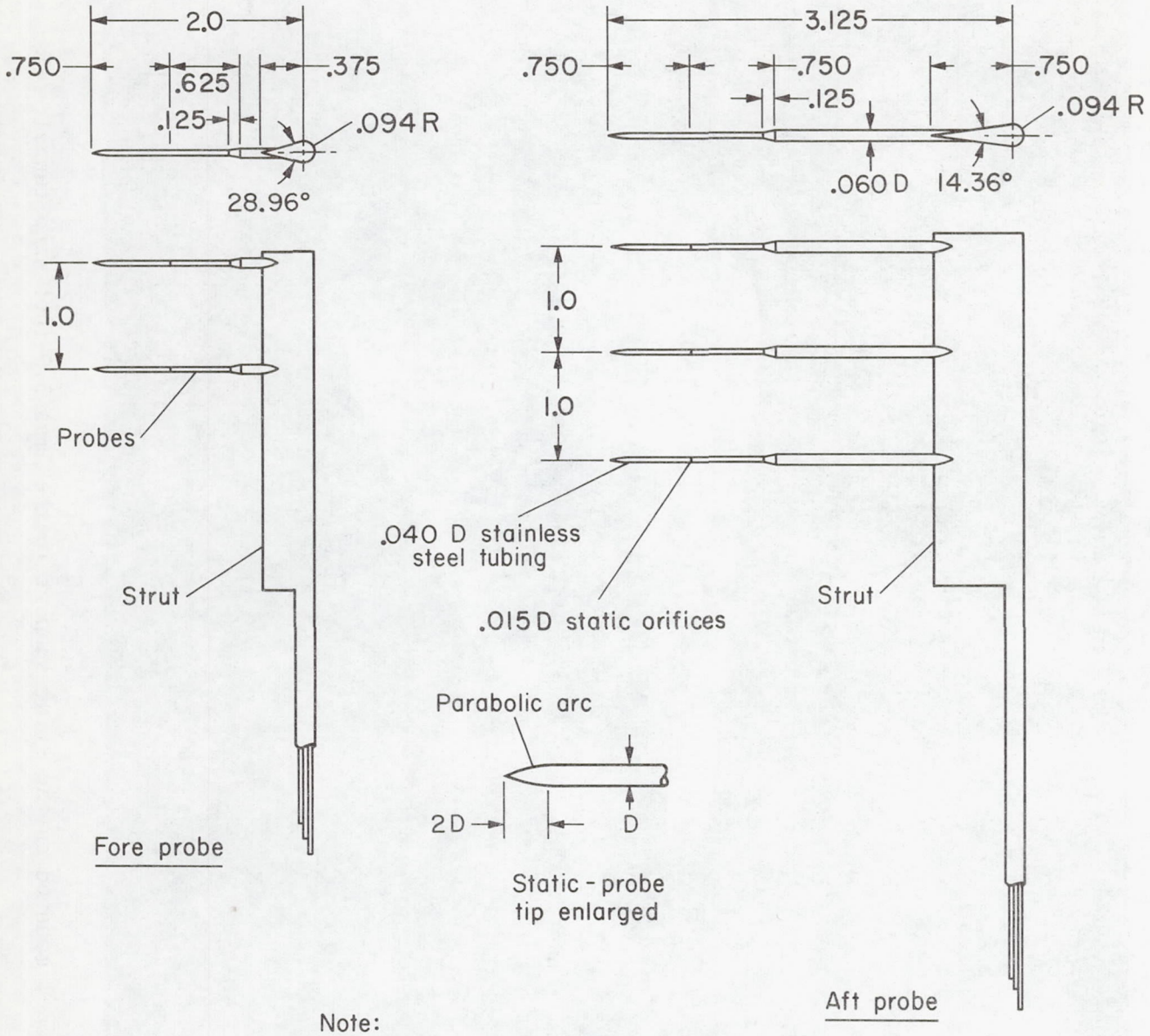

Note:

1 All dimensions in inches.

2 Static-pressure probes shown. Pitot-pressure probes were identical except tubing was cut normal to probes at static orifices.

Figure 2.- Details of pitot- and static-pressure probes.

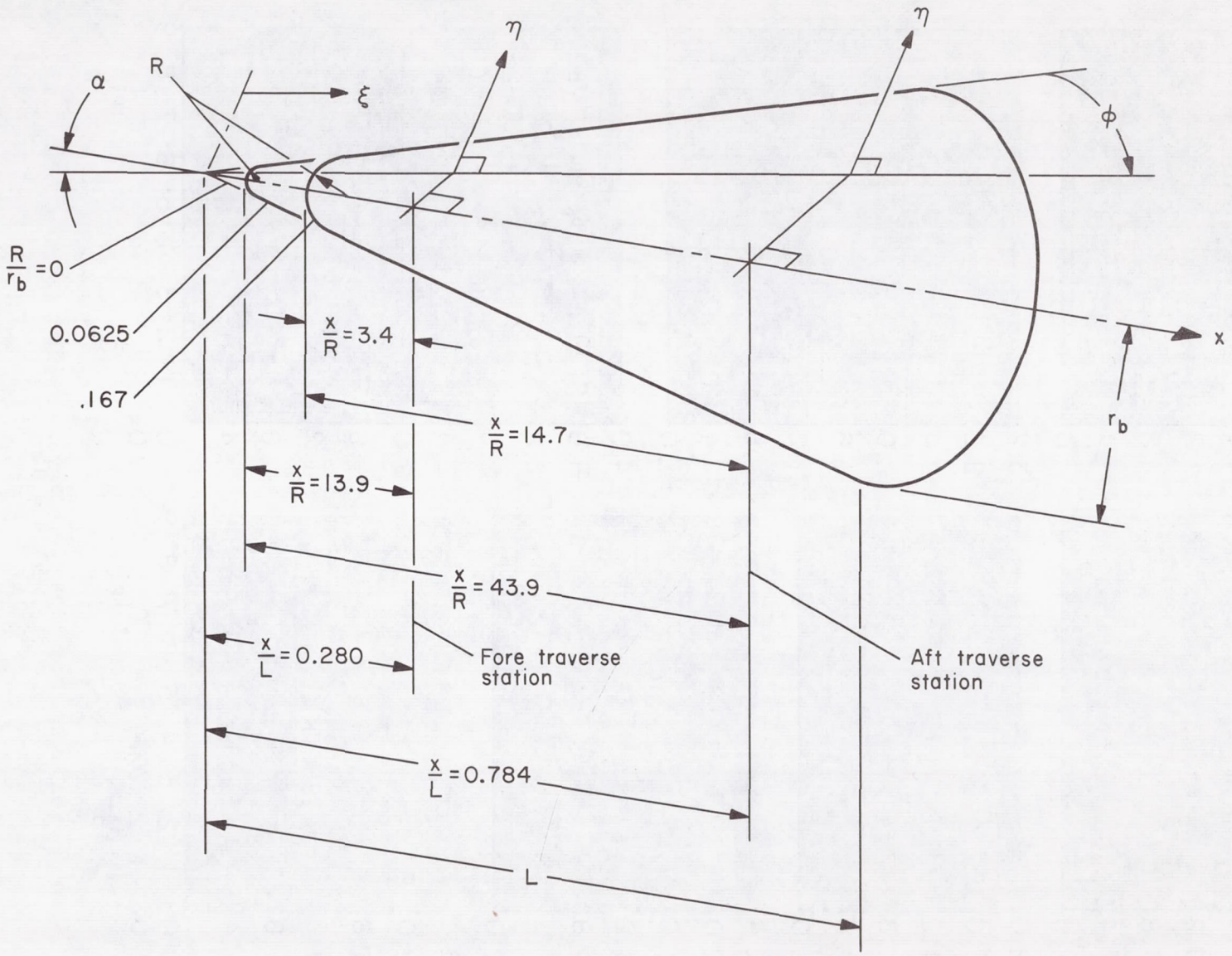

Figure 3.- Geometrical details of the cone traverse stations.

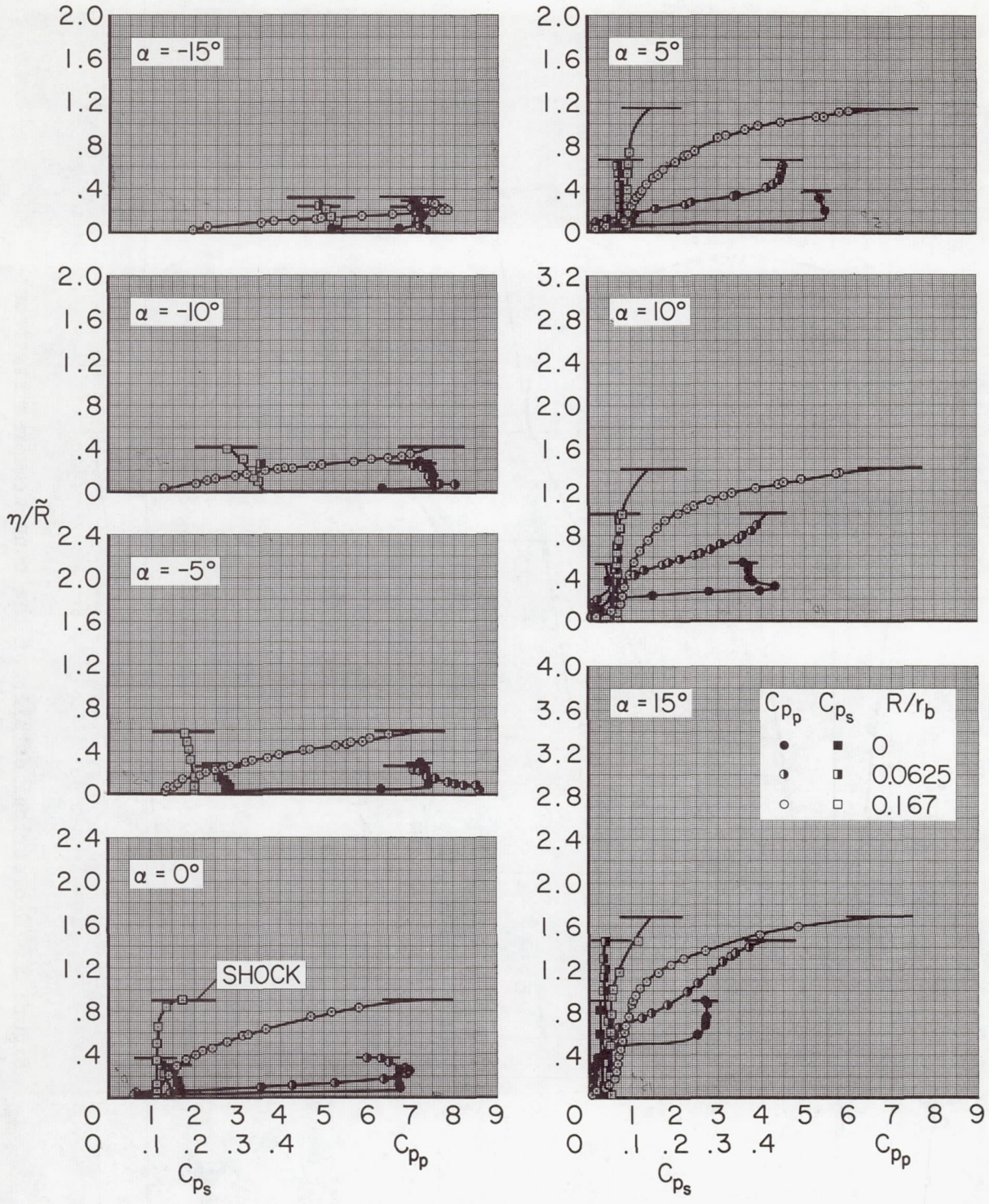

(a) $\phi = 0°$

Figure 4.- Effects of bluntness and angle of attack on the shock-layer properties of the 15° cone at the fore traverse station; x/L = 0.280, M_∞ = 10.6, $\tilde{R}$ = 1 inch, r_b = 6 inches.

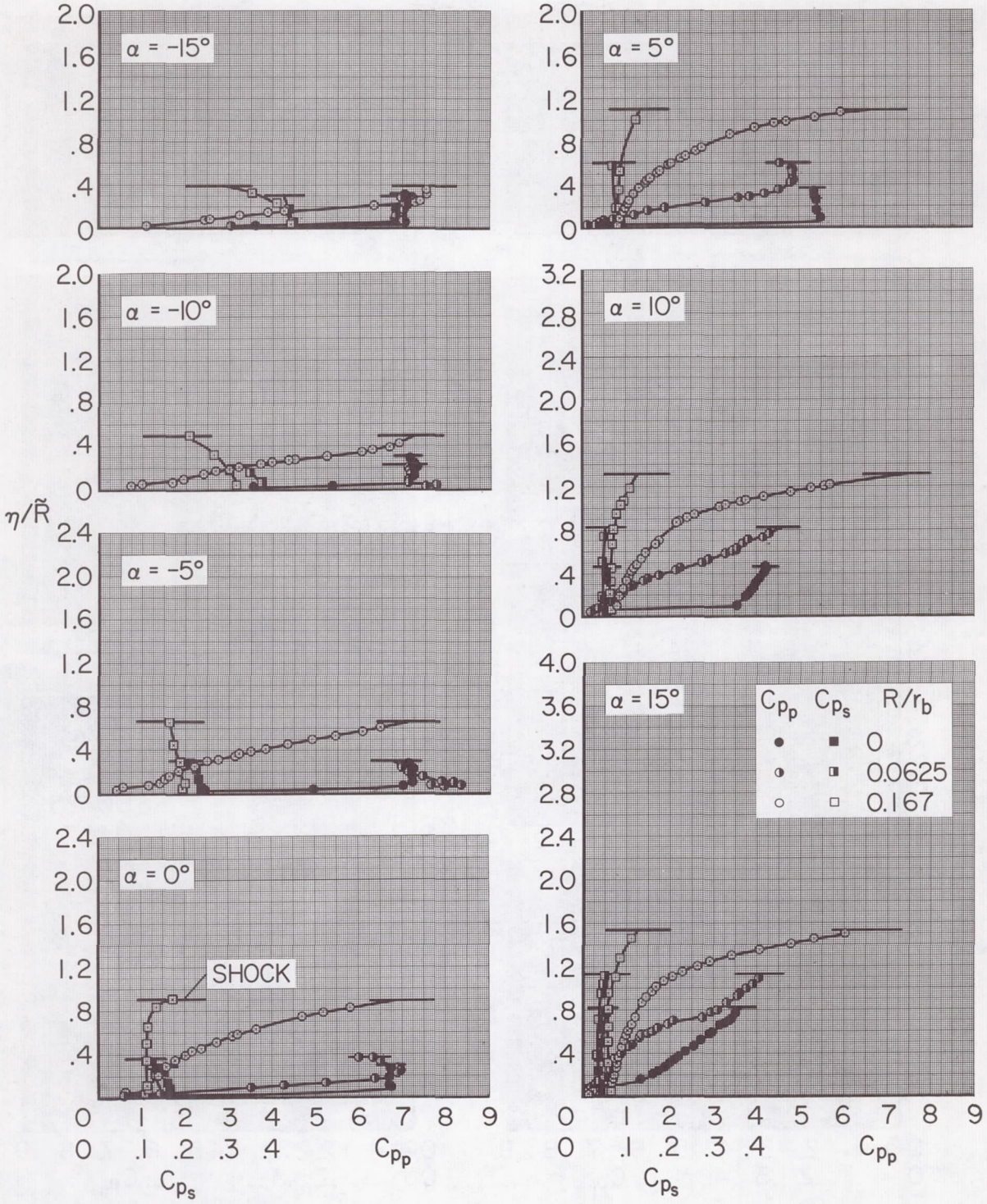

(b) ϕ = 30°

Figure 4.- Continued.

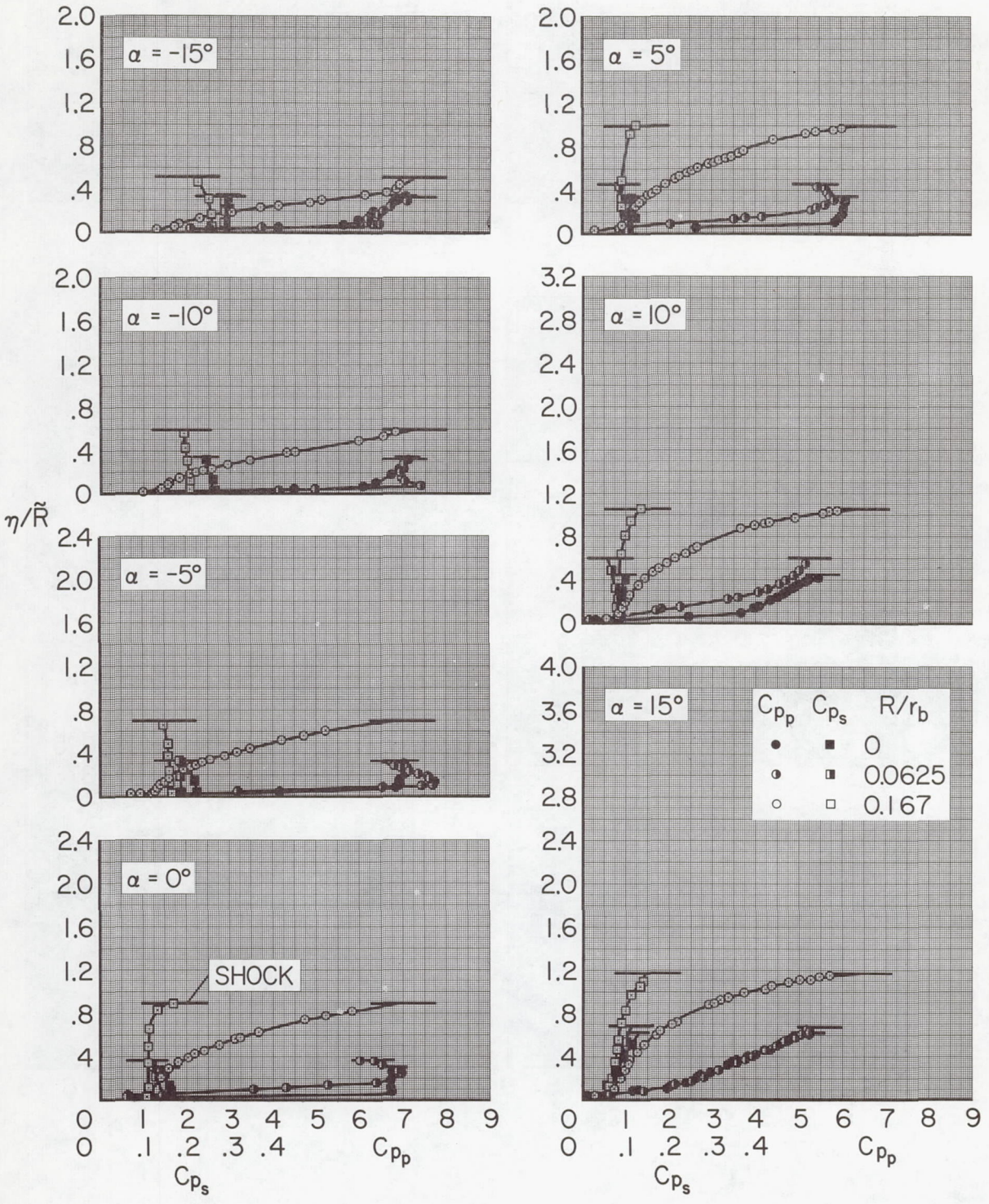

(c) $\phi = 60°$

Figure 4.- Continued.

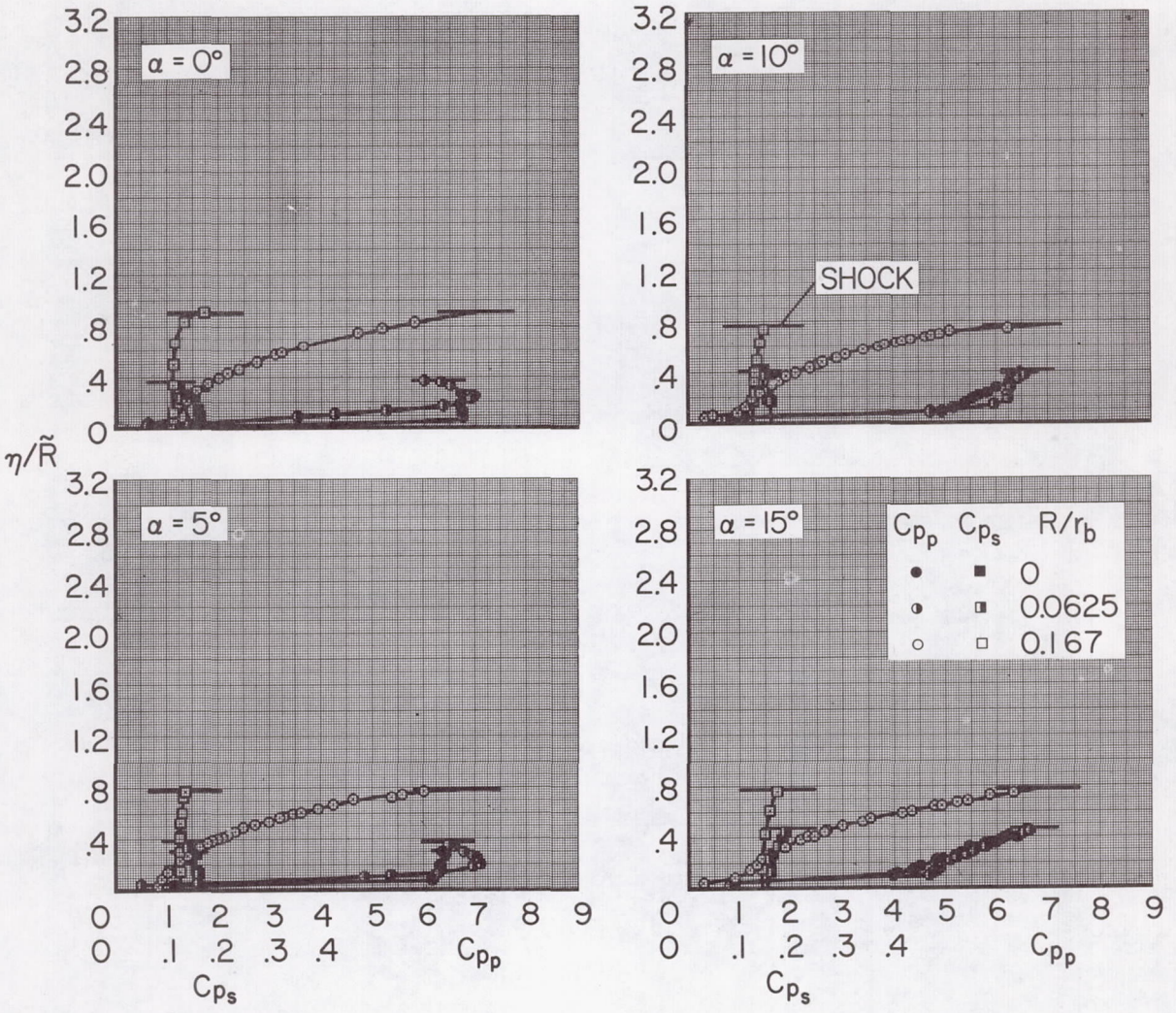

(d) $\phi = 90°$

Figure 4.- Concluded.

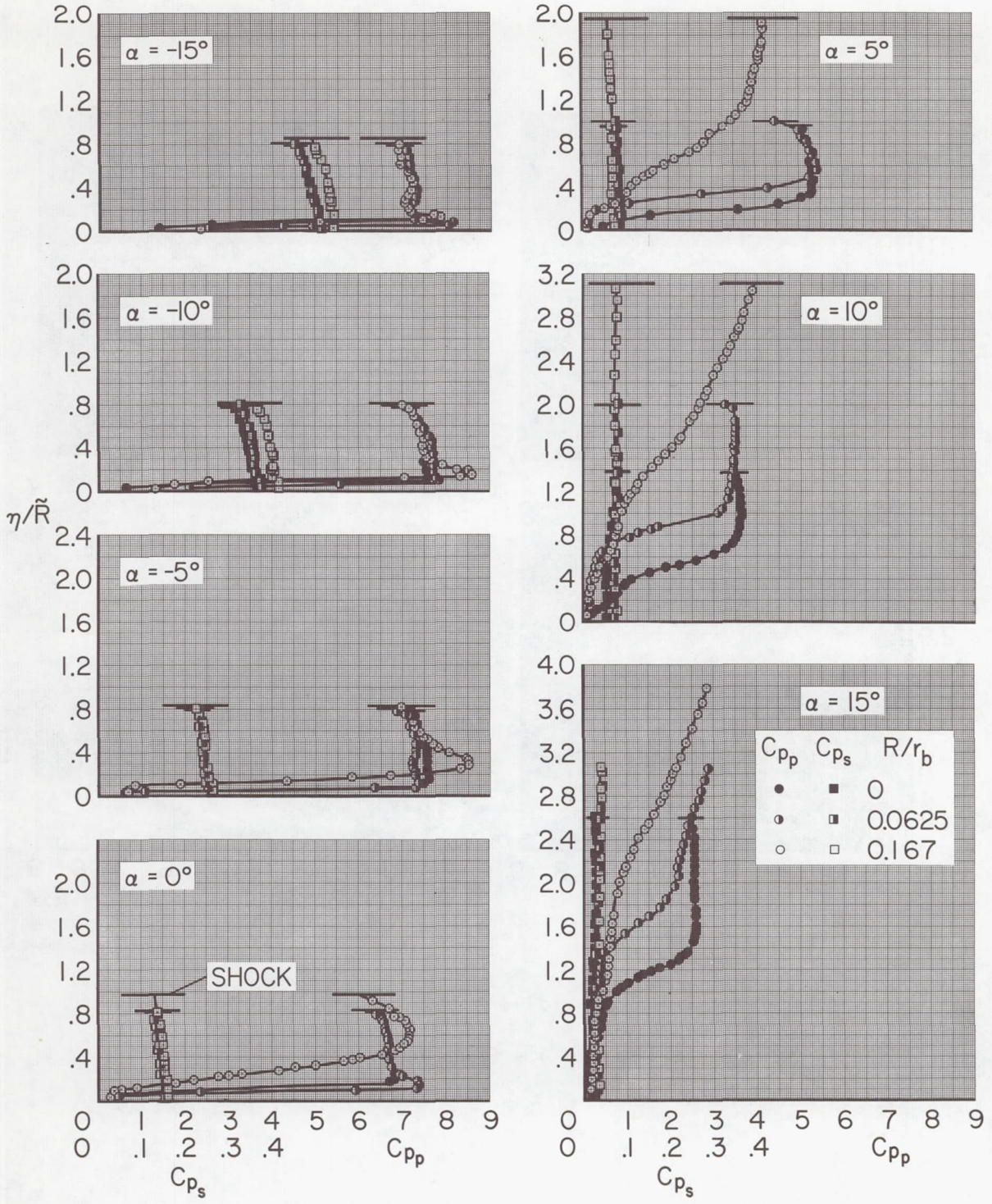

(a) $\phi = 0°$

Figure 5.- Effects of bluntness and angle of attack on the shock-layer properties of the 15° cone at the aft traverse station; x/L = 0.784, M_∞ = 10.6, $\tilde{R}$ = 1 inch, r_b = 6 inches.

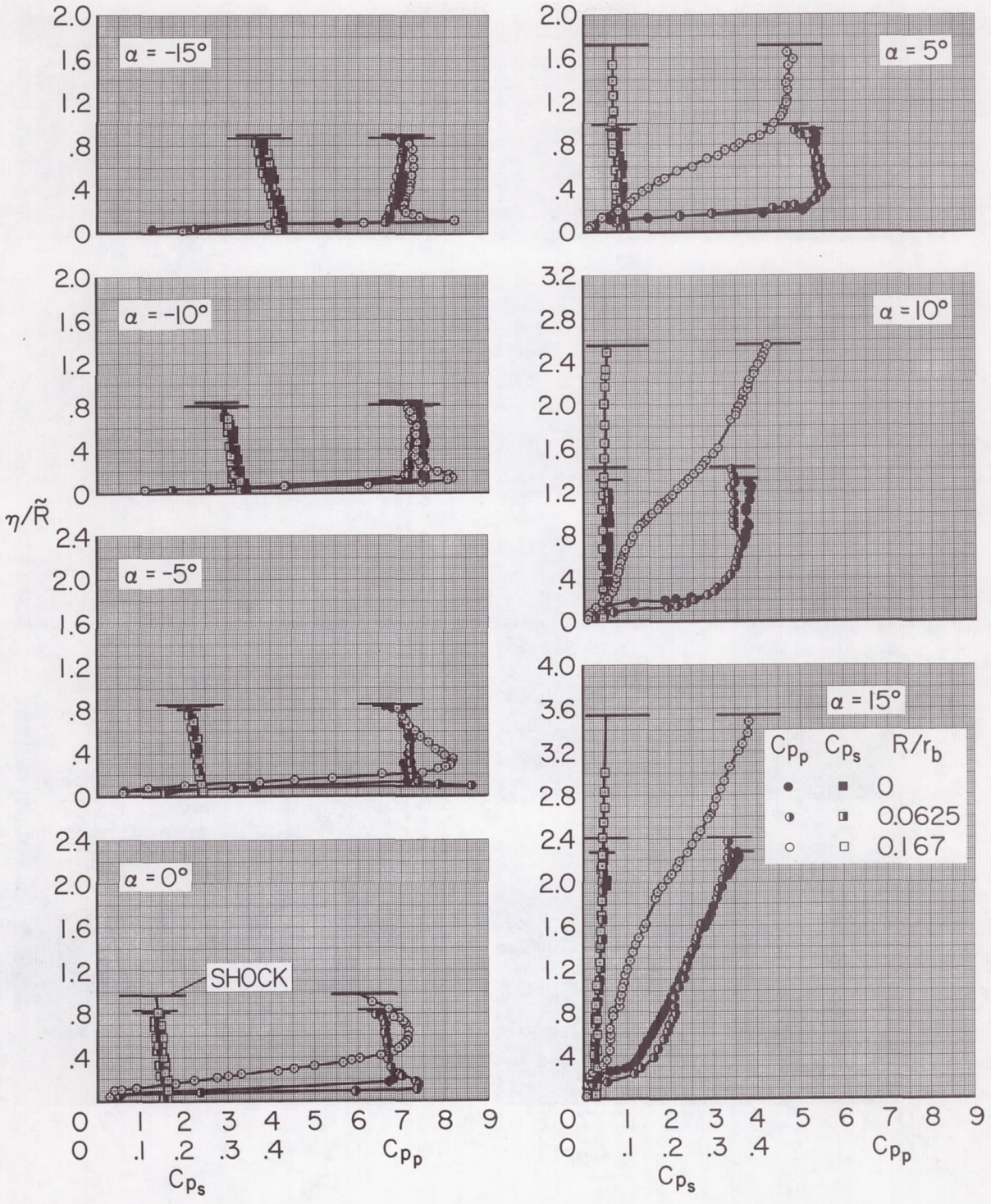

(b) ϕ = 30°

Figure 5.- Continued.

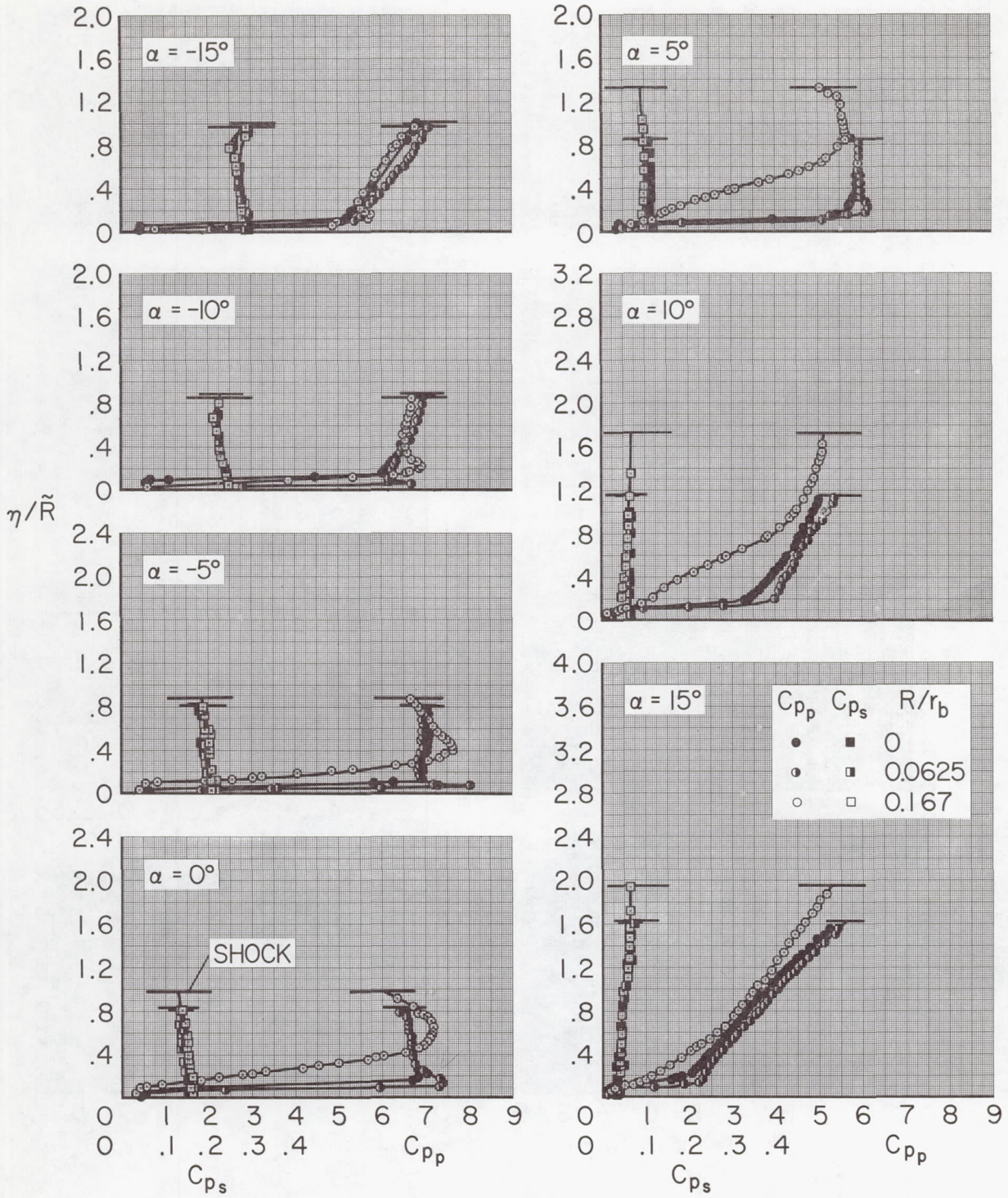

(c) $\phi = 60°$

Figure 5.- Continued.

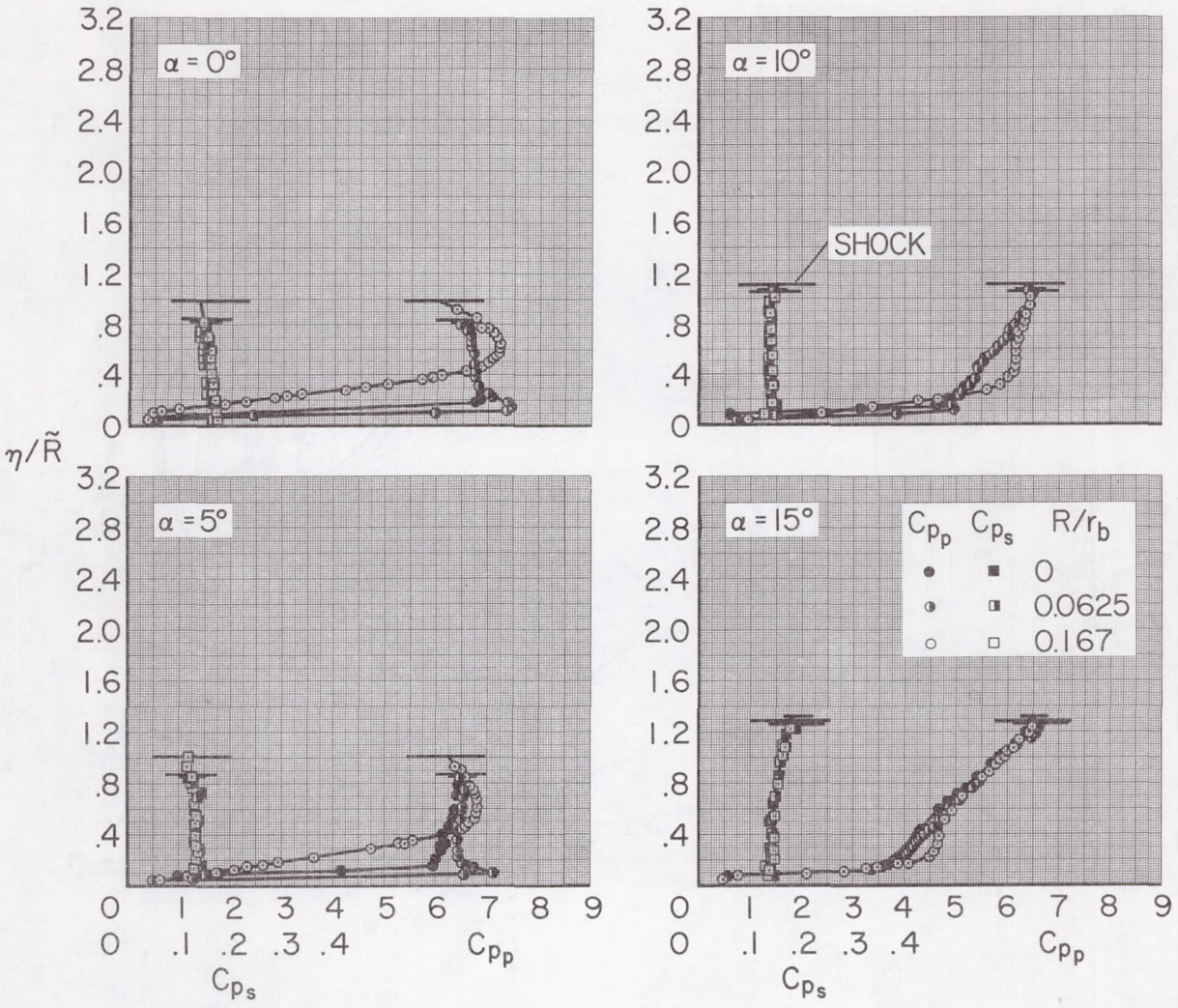

(d) $\phi = 90°$

Figure 5.- Concluded.

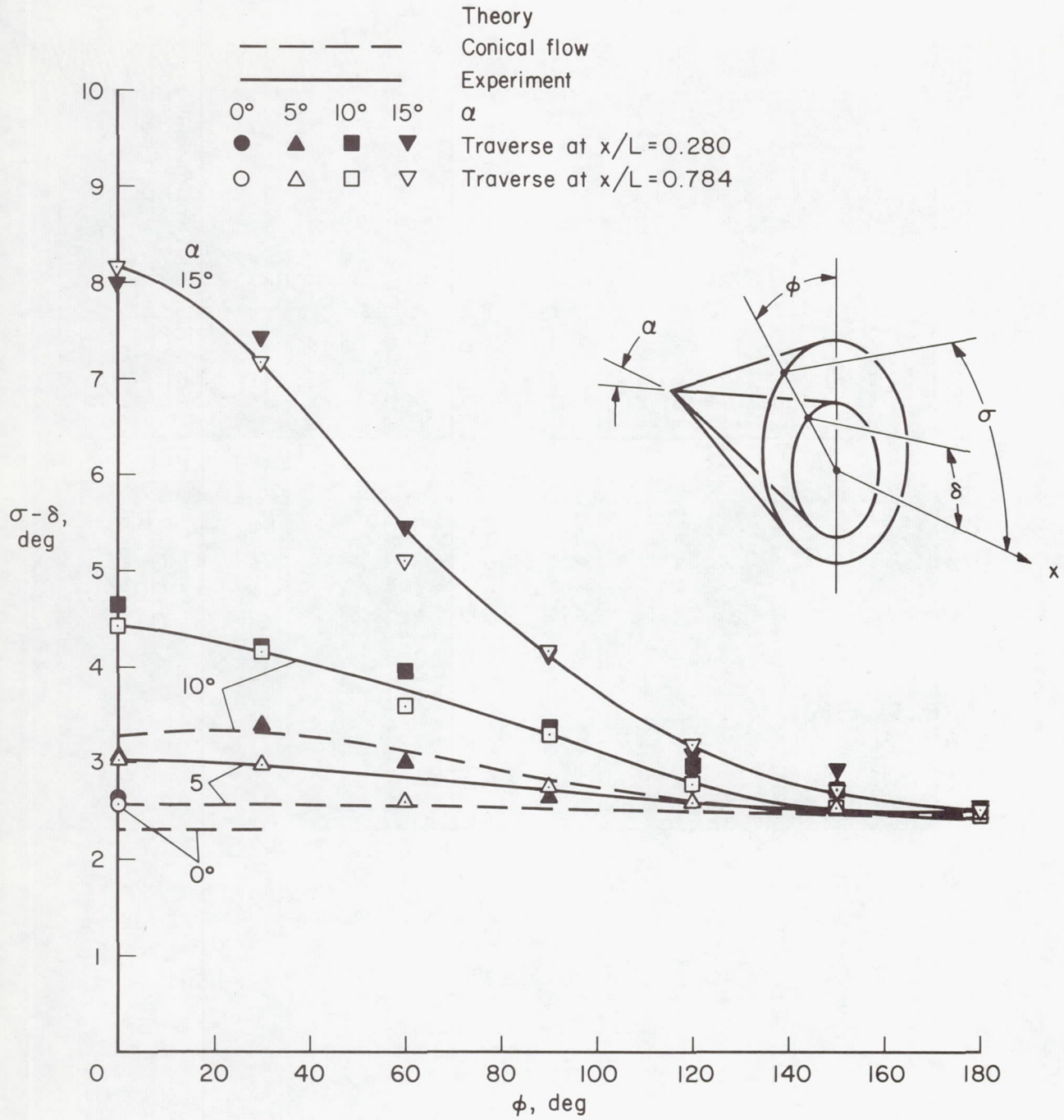

Figure 6.- Comparison of experimental values of $\sigma - \delta$ for the sharp cone with theory; $M_\infty = 10.6$.

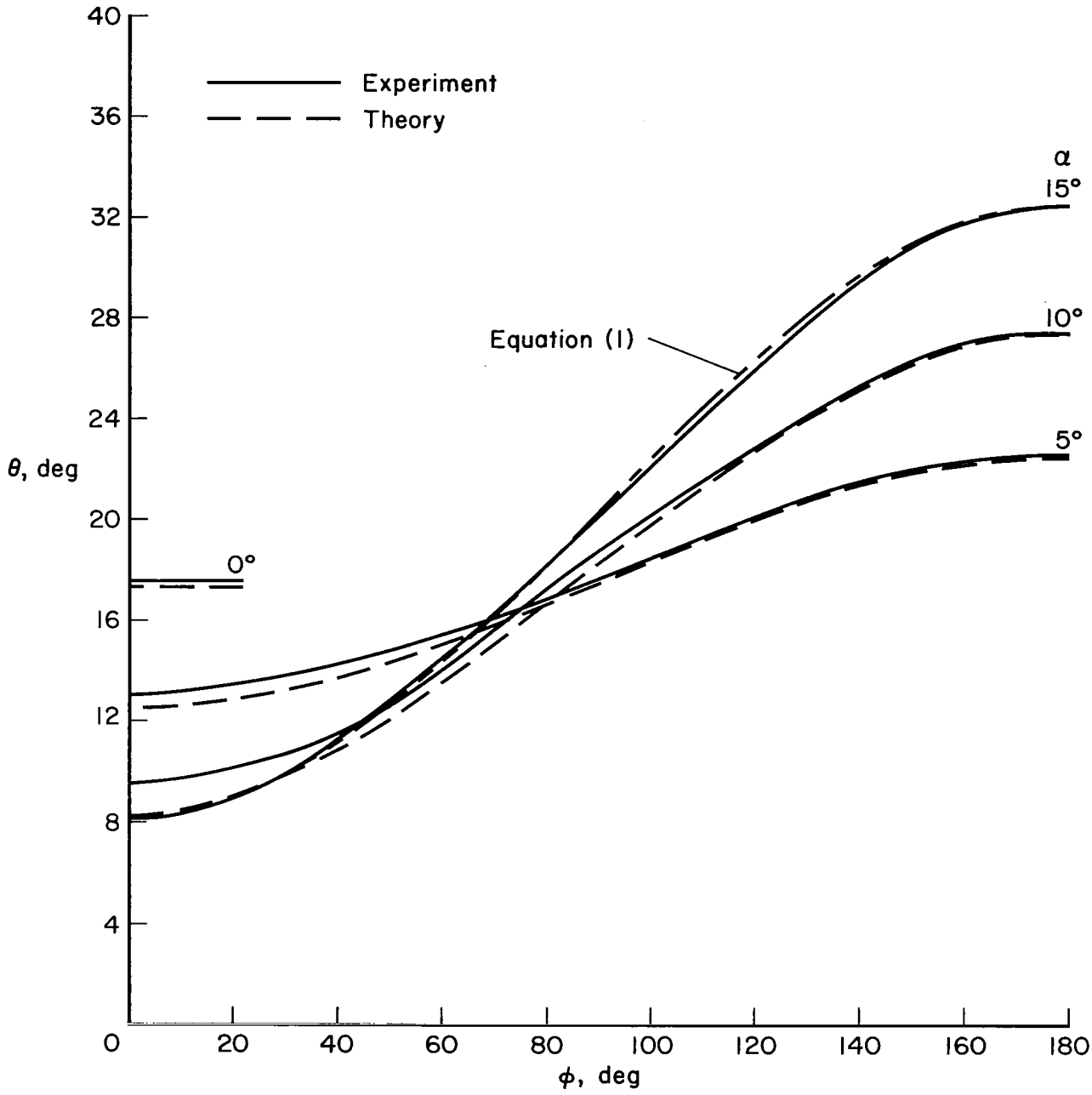

Figure 7.- Comparison of experimental oblique-shock angles of the sharp cone with theory; $M_\infty = 10.6$.

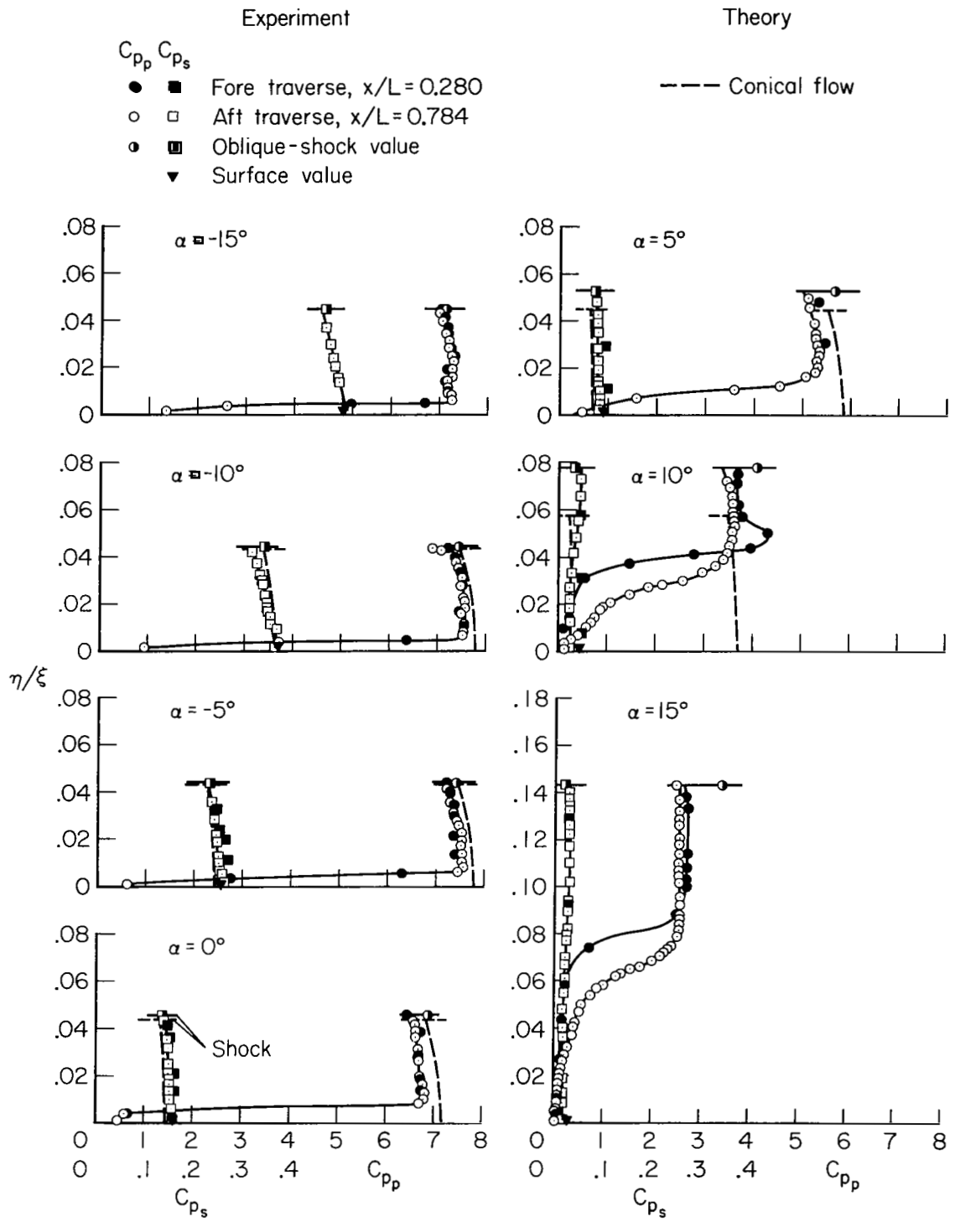

(a) $\phi = 0°$

Figure 8.- Comparison of sharp-cone shock-layer properties with theory; $M_\infty = 10.6$.

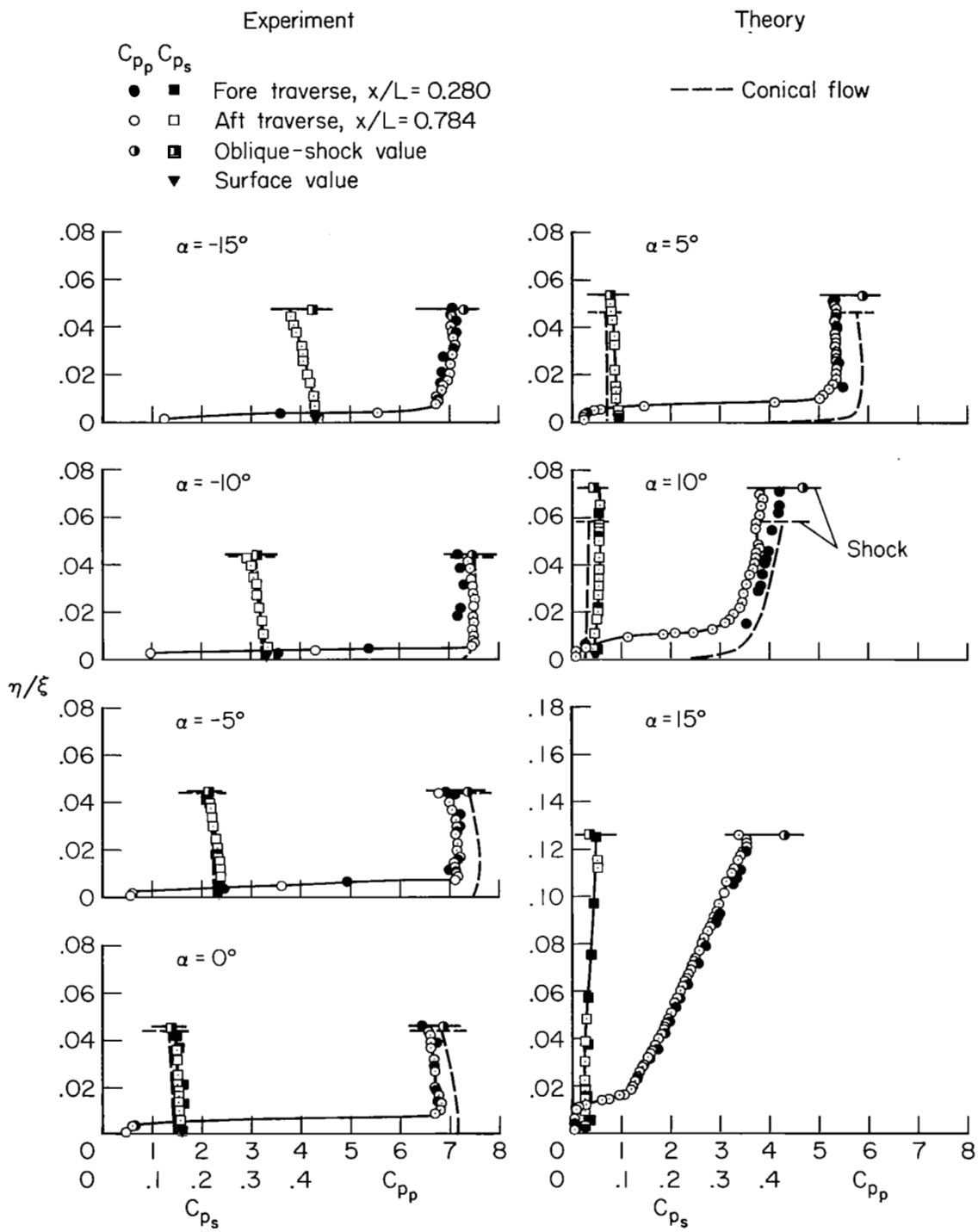

(b) $\phi = 30°$

Figure 8.- Continued.

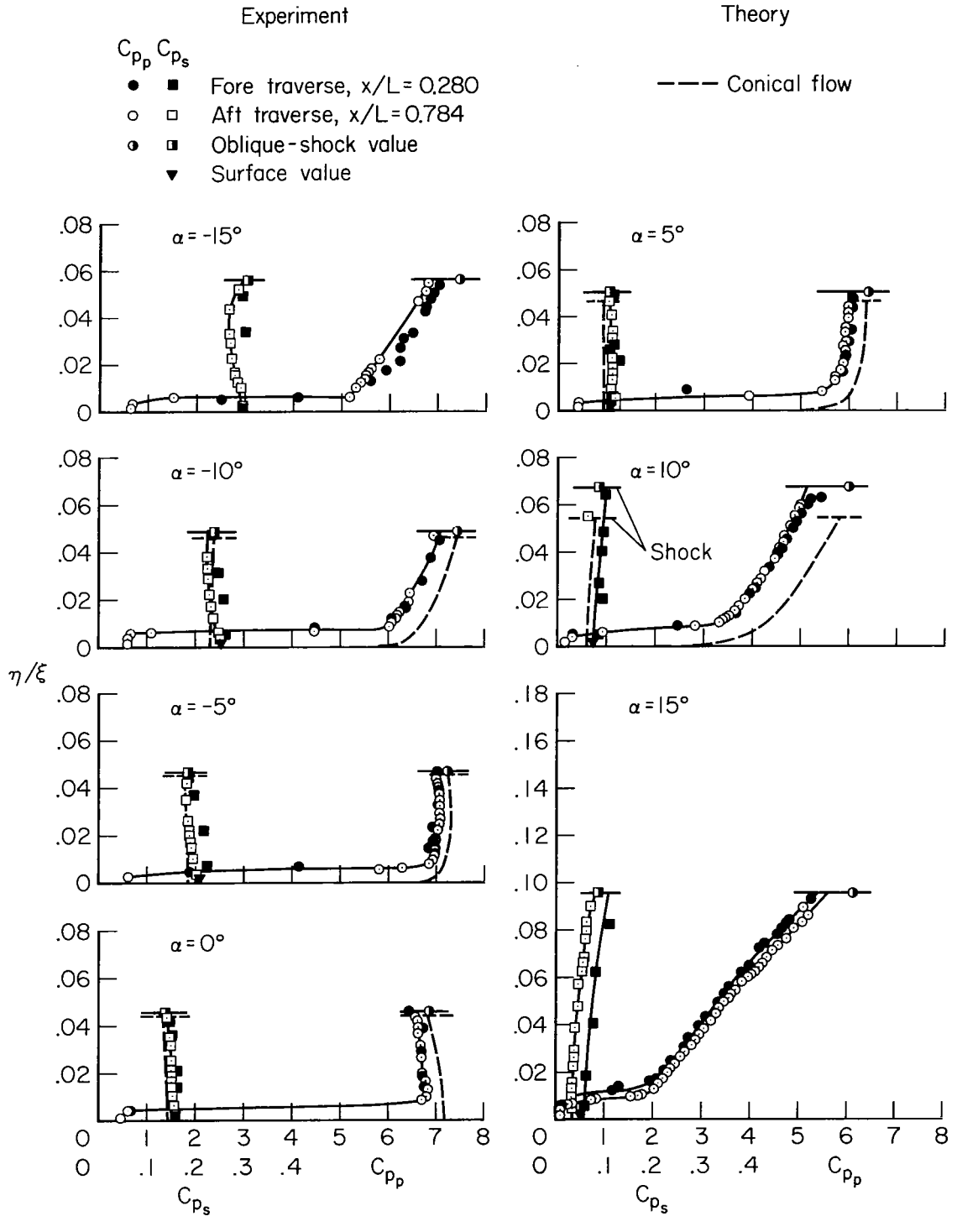

(c) ϕ = 60°

Figure 8.- Continued.

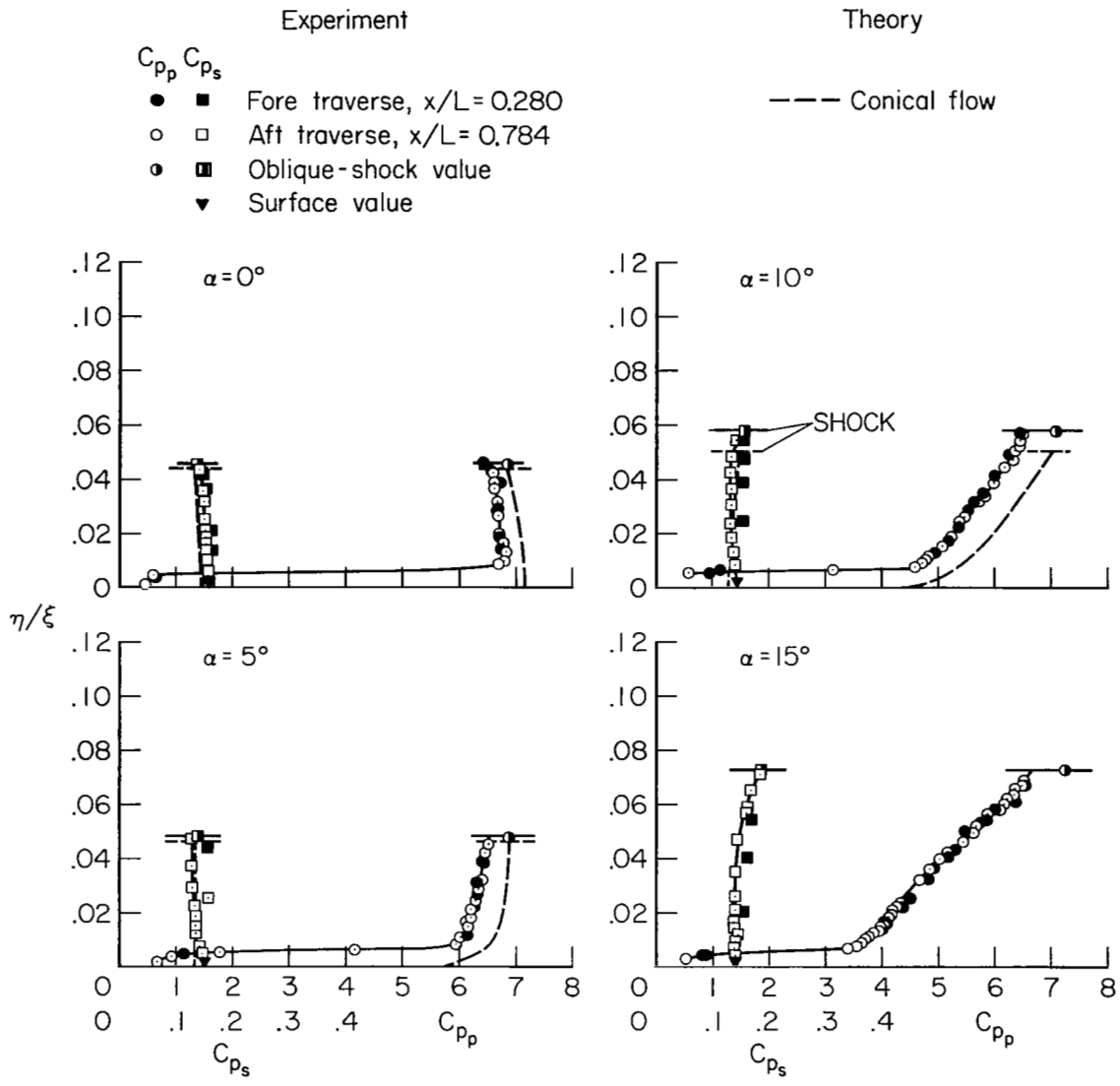

(d) ϕ = 90°

Figure 8.- Concluded.

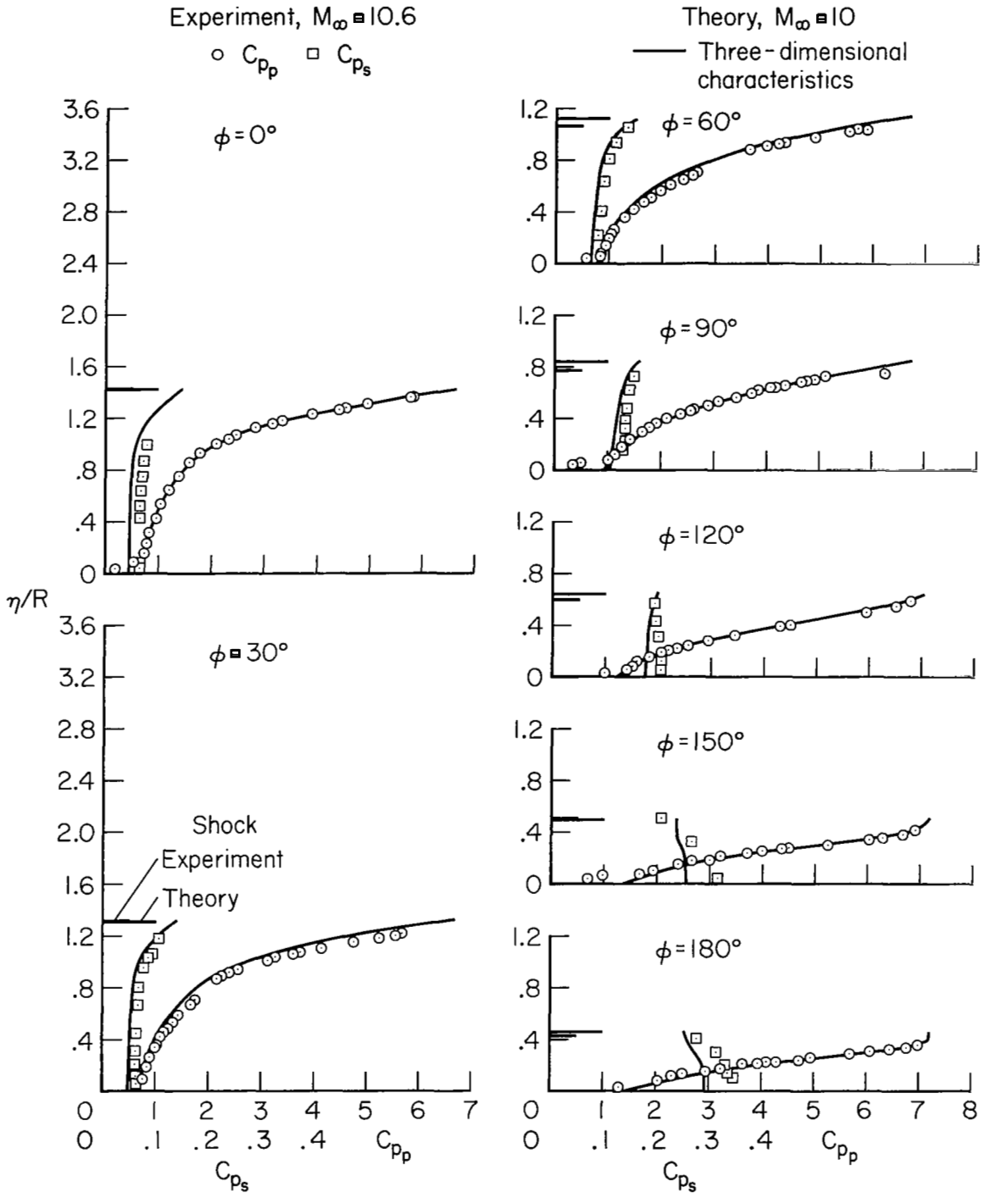

(a) Fore-traverse station, x/R = 3.4.

Figure 9.- Comparison of blunted-cone shock-layer properties with three-dimensional characteristics theory at $\alpha = 10°$, $R/r_b = 0.167$.

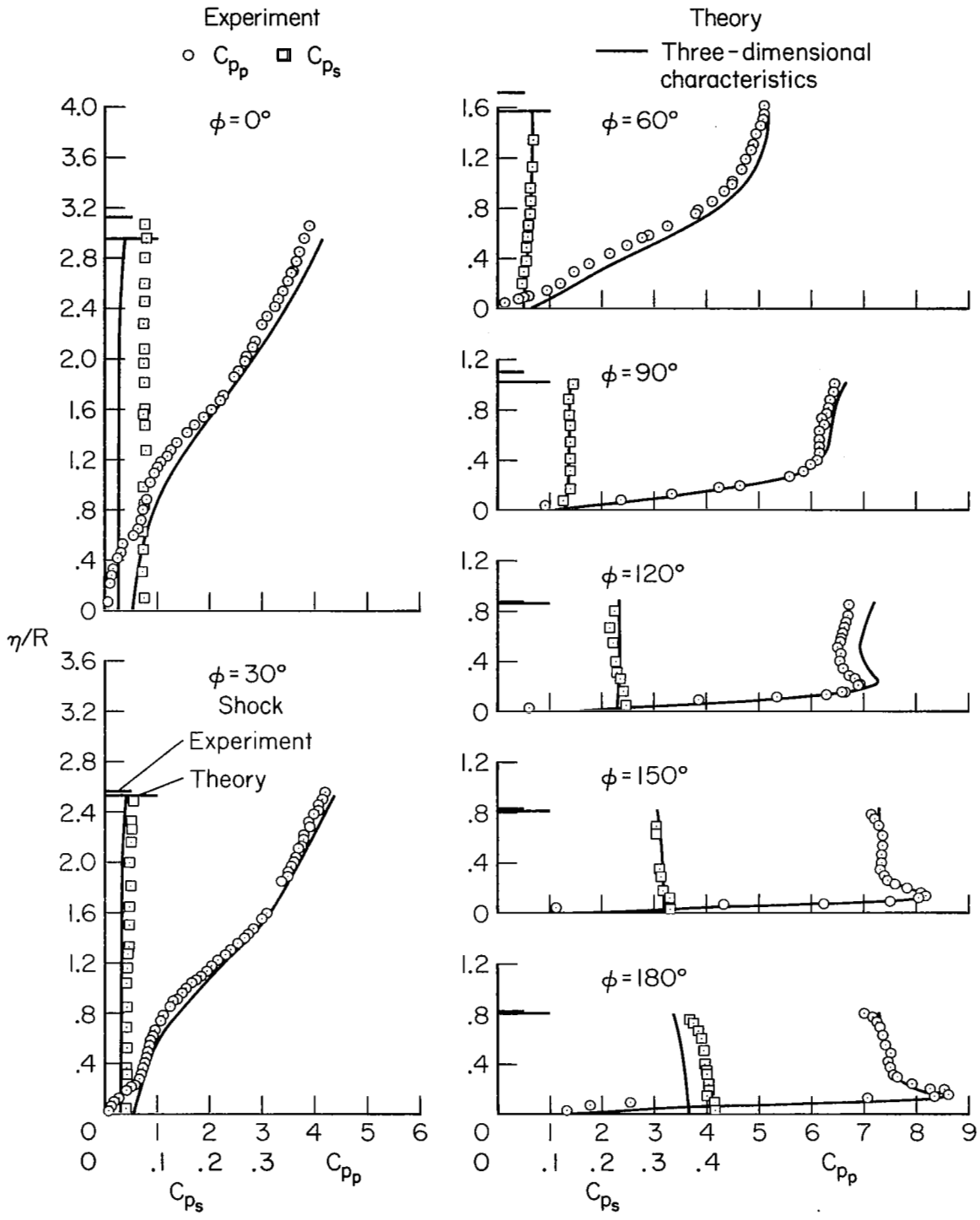

(b) Aft-traverse station, x/R = 14.7.

Figure 9.- Concluded.

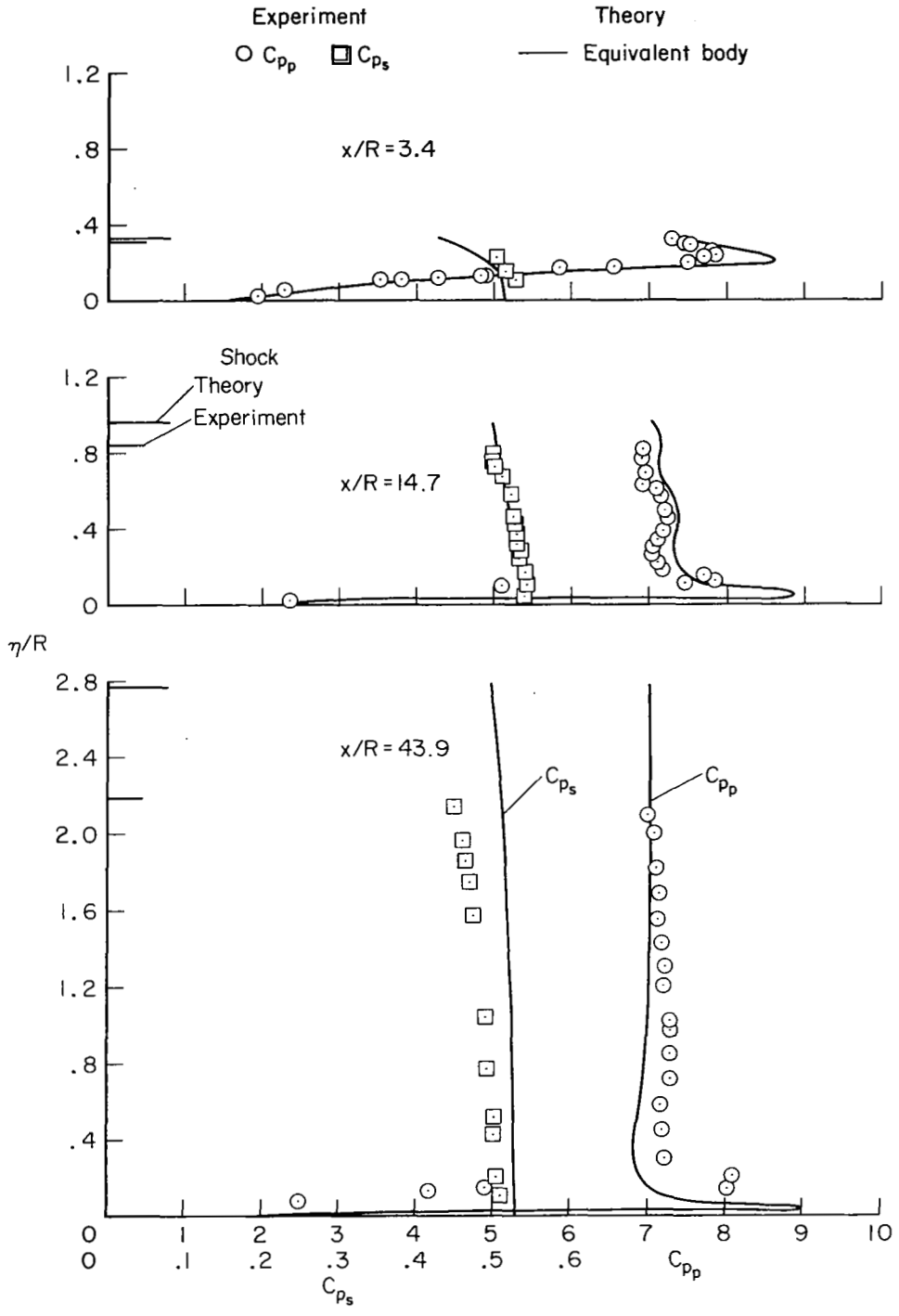

(a) $\alpha = -15°$

Figure 10.- Comparison of blunted-cone shock-layer properties with equivalent-body theory for $\phi = 0°$, $M_\infty = 10.6$.

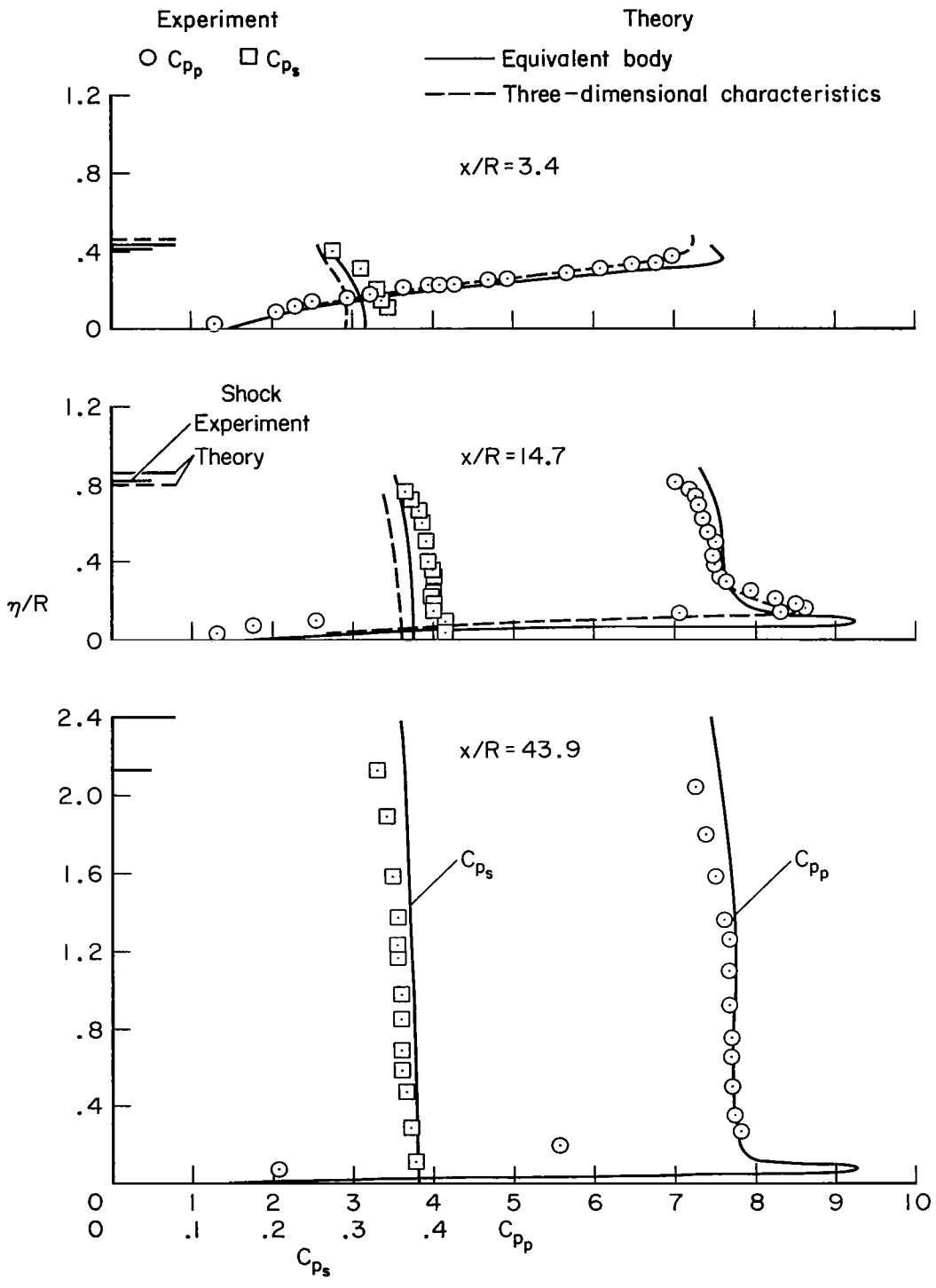

(b) $\alpha = -10°$

Figure 10.- Continued.

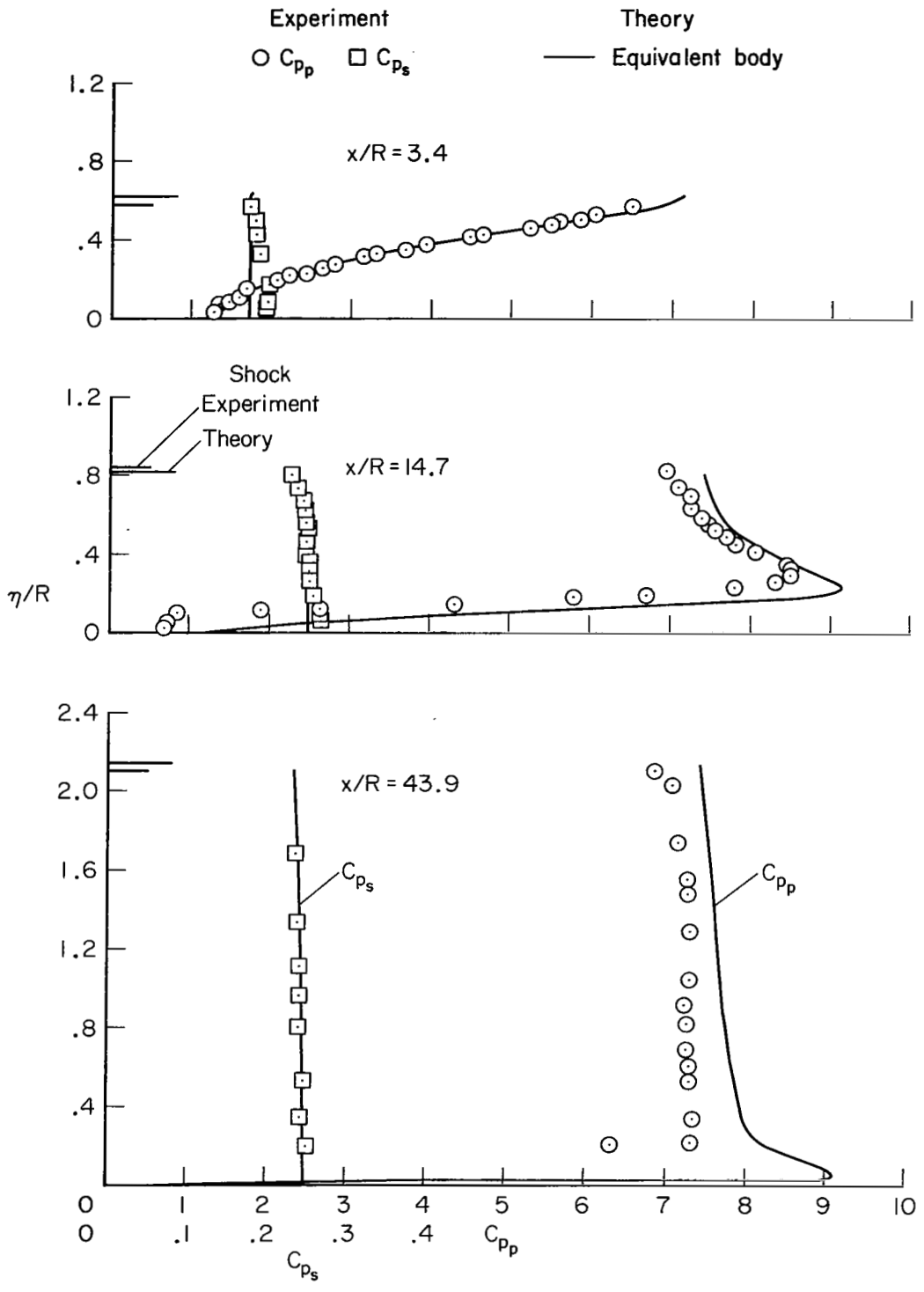

(c) $\alpha = -5°$

Figure 10.- Continued.

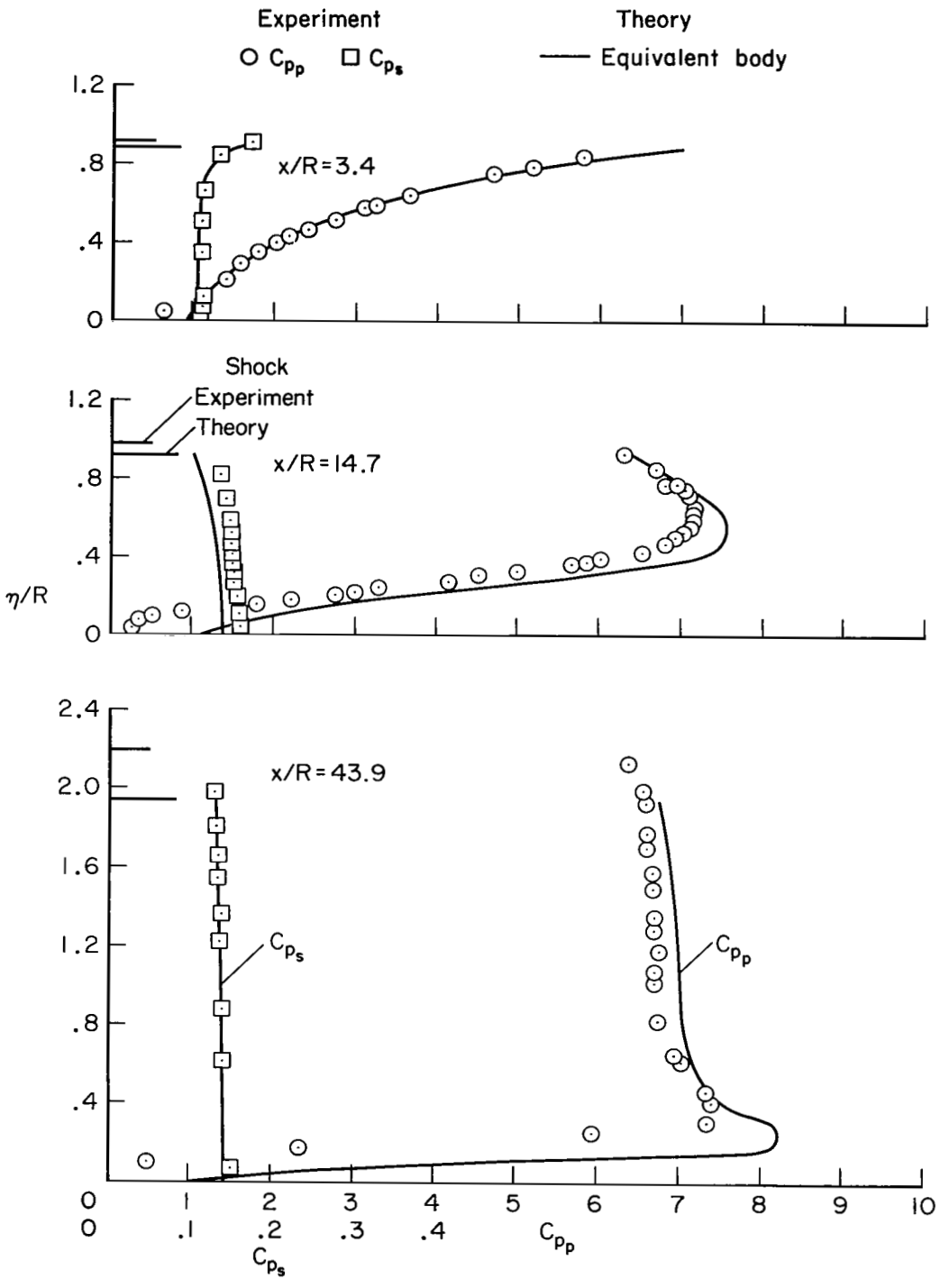

(d) $\alpha = 0°$

Figure 10.- Continued.

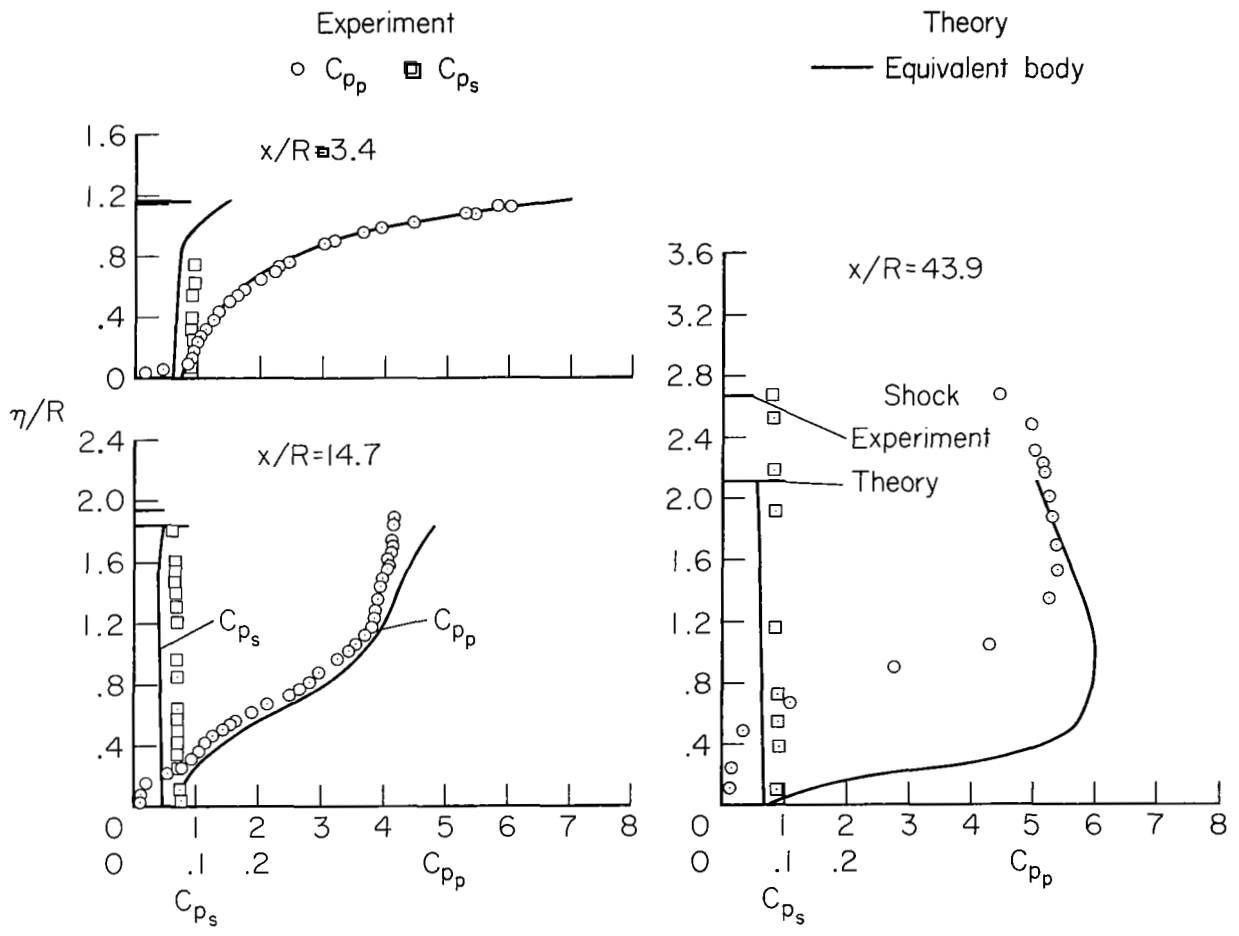

(e) $\alpha = 5°$

Figure 10.- Continued.

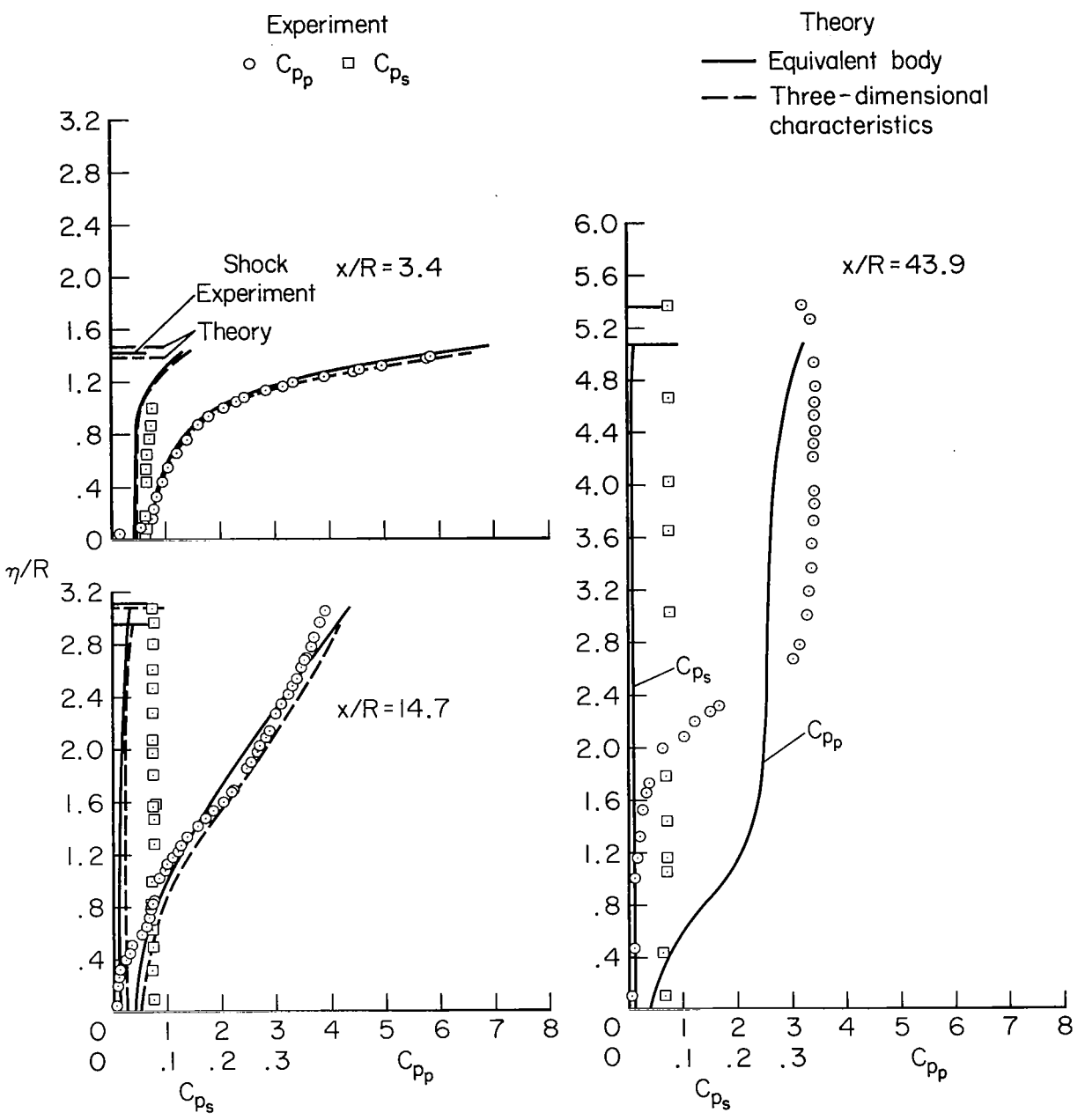

(f) $\alpha = 10°$

Figure 10.- Continued.

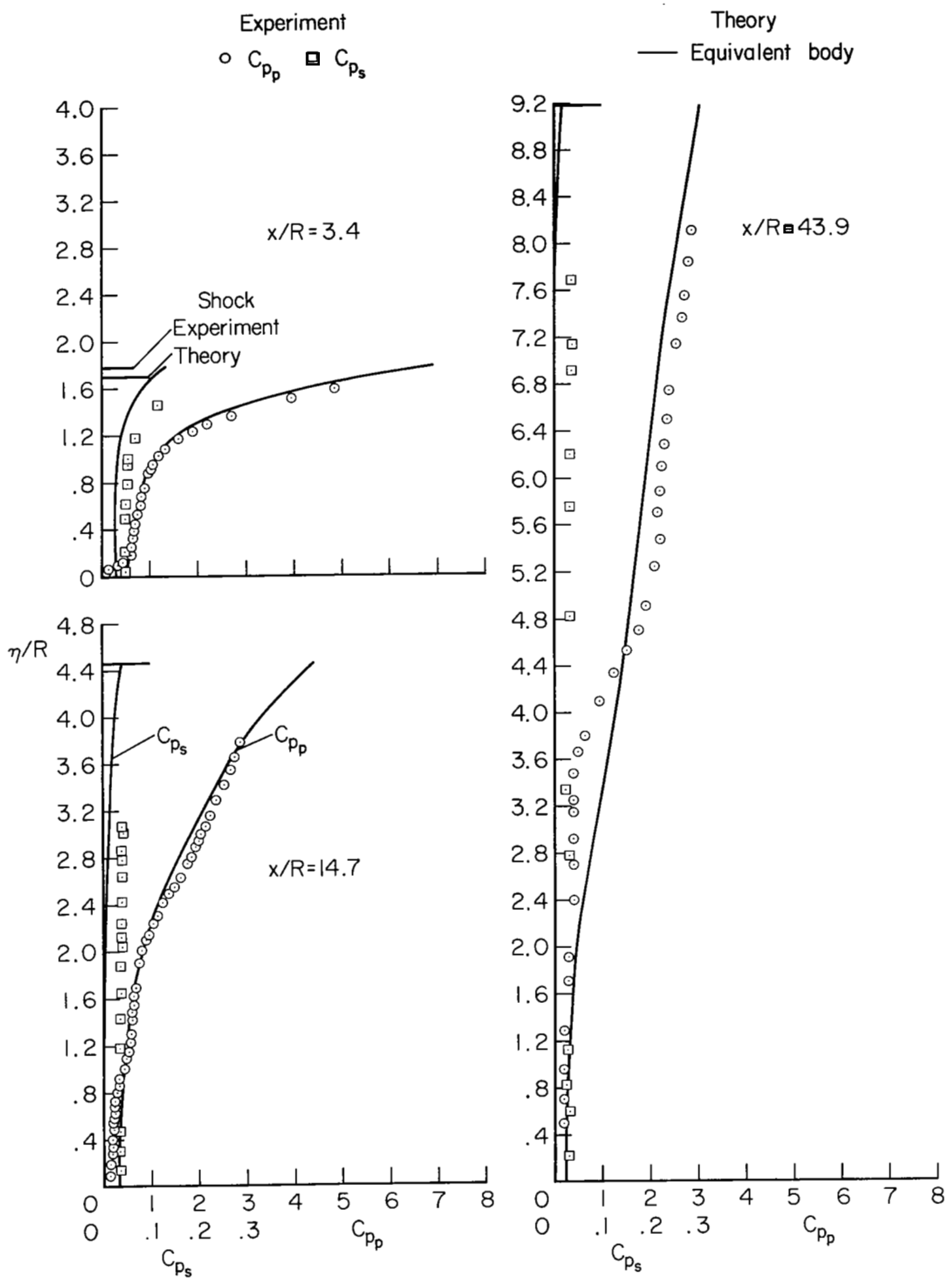

(g) α = 15°

Figure 10.- Concluded.

NASA-Langley, 1968 —— 1 A-3035